

AN ABSTRACT OF THE THESIS OF

John R. Toth for the degree of Master of Science
in Oceanography presented on 3 February 1977

Title: DEPOSITION OF SUBMARINE HYDROTHERMAL MANGANESE AND IRON, AND
EVIDENCE FOR HYDROTHERMAL INPUT OF VOLATILE ELEMENTS TO THE
OCEAN

Abstract approved:

Redacted for Privacy

Jack Dymond

The chemical and mineralogical analysis of manganese-rich and iron rich oxide crusts, of probable hydrothermal origin, from several locations on active spreading centers and seamounts in the Pacific and Atlantic indicate that these crusts originate from a uniform depositional process. These crusts are characterized by extreme Fe/Mn ratios, Fe and Si contents which co-vary, generally very low concentrations of most trace metals and the rare earth elements, and variable contents of Zn and the volatile elements Hg, As and Sb. These compositions can be accounted for by the fractional precipitation of Fe, SiO₂ and Mn and possible incorporation of Zn, As, Sb and Hg from hydrothermal solutions, and adsorption of minor amounts of Co, Cu, Ni, Pb, Ba and rare earth elements from seawater.

Mineralogical analysis by ultra-slow scan X-ray diffraction show the manganese-rich crusts to be composed of very pure, highly crystalline birnessite or todorokite. Iron-rich crusts consist of either amorphous hydrated iron oxide and silica or iron-rich, low aluminum nontronite.

Analysis of a suite of ferromanganese coatings formed on ocean-ridge outcroppings of basalt and a number of Pacific manganese nodules indicate that ferromanganese coatings are enriched in Fe and Si and depleted in trace metals relative to nodules, and are similar in chemical composition to East Pacific Rise metalliferous sediments. The mineralogy of the ferromanganese coatings is dominated by poorly crystalline δMnO_2 and the accessory minerals phillipsite, quartz and calcite.

The similarity of the ferromanganese coatings to metalliferous sediments suggests that they have a common origin. It is believed that most of the Fe, SiO_2 and Mn entering seawater in hydrothermal solutions precipitates as colloidal SiO_2 and hydrated Fe and Mn oxides which are advected by bottom currents and deposited as these coatings and sediments. Trace element contents in these deposits result from adsorption from seawater onto the Fe and Mn colloids during advection.

Deposition of Submarine Hydrothermal Manganese
and Iron, and Evidence for Hydrothermal Input
of Volatile Elements to the Ocean

by

John R. Toth

A THESIS

submitted to

Oregon State University

in partial fulfillment of
the requirements for the
degree of

Master of Science

June 1977

APPROVED:

Redacted for Privacy

Associate Professor of Oceanography
in charge of major

Redacted for Privacy

Dean of School of Oceanography

Redacted for Privacy

Dean of Graduate School

Date thesis is presented on February 3, 1977

Typed by Margie Wolski for John R. Toth

ACKNOWLEDGEMENTS

I would like to thank Dr. Jack Dymond, my advisor, for his assistance and comments on this work. Special thanks go to Dr. James Ingle for his interest and help in analytical matters. I am also grateful for the comments by the other members of my committee, Drs. Erwin Suess, E. Julius Dasch and John B. Corliss.

I extend my appreciation to Drs. Robert Scott, Helmut Beiersdorf, Michel Hoffert, Willard Moore and David Piper for providing samples for this study. Radiation counting facilities and assistance were kindly provided by Dr. Vern Smith.

I am indebted to Ronald Stillinger and Christin Chow for assistance in technical matters and beyond. Valuable discussions with Mitch Lyle are also appreciated. Others without whom this work could not have been completed are Nancy, Jim, Chris, Simon, Marty and Cliff.

I wish to thank Margie Wolski for typing this manuscript and Peggy Lorraine for the excellent drafting of figures.

This work was supported in part by a graduate research fellowship from the International Nickel Company.

TABLE OF CONTENTS

	<u>Page</u>
INTRODUCTION	1
Evidence of Oceanic Hydrothermal Activity	2
Chemical Interactions in Hydrothermal Systems	3
Volatile Elements	4
SAMPLES	6
Hydrothermal Crusts	6
Ferromanganese Coatings and Nodules	7
METHODS OF ANALYSIS	8
Sample Preparation	8
Atomic Absorption Spectroscopy	9
Cold Vapor AAS of Mercury	10
Instrumental Neutron Activation Analysis	13
X-ray Diffraction Analysis	14
MINERALOGY	15
CHEMISTRY RESULTS	18
Major and Minor Elements	18
Rare Earth Elements	29
Volatile Elements	37
DISCUSSION	45
Hydrothermal Crusts: Major Element Composition	45
Hydrothermal Crusts: Minor Element Composition	48
Ferromanganese Coatings and Nodules	55
CONCLUSIONS	58
BIBLIOGRAPHY	61
APPENDIX I	68
APPENDIX II	75
APPENDIX III	79

LIST OF TABLES

<u>Table</u>		<u>Page</u>
1	Operating Parameters for Atomic Absorption Spectroscopy	11
2	Mineralogy Results from X-ray Diffraction Analysis	17
3	Cerium Anomalies	38

LIST OF FIGURES

<u>Figure</u>		<u>Page</u>
1	Ternary diagram of Fe vs. Mn vs. Co + Ni + Cu	19
2	Ternary diagram of Fe vs. Mn vs. Si	21
3	Plot of Si vs. Al	23
4	Ternary diagrams of Ni vs. Cu vs. Co and Ni vs. Cu vs. Zn	25
5	Ternary diagram of Fe vs. Mn vs. Ba	26
6	Ternary diagram of factor analysis results	28
7	Shale normalized REE patterns of ferromanganese coatings and nodules	31
8	Shale normalized REE patterns of hydrothermal crusts	32
9	Seawater normalized REE patterns of TAG hydrothermal crusts	34
10	Shale normalized REE patterns of AMPH D6 deposits and Fe-Mn impregnated sediment	35
11	Shale normalized REE patterns of average seawater, tholeiites and marine sediments	36
12	Plot of La vs. Ce	39
13	Plot of As vs. Sb	40
14	Plot of Fe vs. As	42
15	Ternary diagram of Fe vs. Mn vs. Hg	43
16	Processes involved in deposition of hydrothermal Fe, Mn and SiO ₂	60a

DEPOSITION OF SUBMARINE HYDROTHERMAL MANGANESE
AND IRON, AND EVIDENCE FOR HYDROTHERMAL
INPUT OF VOLATILE ELEMENTS TO THE OCEAN

INTRODUCTION

Recent discoveries of thick, manganese-rich and iron-rich crusts near active spreading centers of the oceans have helped confirm the existence of the large scale juvenile input of manganese and iron to the oceans by submarine hydrothermal processes. These unusual deposits appear to accumulate 2 to 3 orders of magnitude faster than more typical ferromanganese deposits, have very low trace metal and ^{230}Th content, and, in many cases, anomalous $^{234}\text{U}/^{238}\text{U}$ values (M. R. Scott et al., 1974; Moore and Vogt, 1975; Piper et al., 1975). These characteristics rule out normal seawater as the source of elements in the deposits, but are consistent with formation by direct precipitation from iron and manganese-rich submarine hot springs.

Although deposits of probable marine hydrothermal origin have been studied individually by several researchers, this study, of deposits from several geographic locations, is an attempt to determine whether their chemical and mineralogical properties can be accounted for by a consistent theory of hydrothermal deposition.

The data used for this study consists of the results from the chemical and mineralogical analysis of seven thick manganese-rich "hydrothermal" crusts from 1) the Galapagos Spreading Center, 2) the Trans-Atlantic Geotraverse (TAG) hydrothermal field of the Mid-Atlantic Ridge, and 3) the French-American Mid-Ocean Undersea Study (FAMOUS) dive area of the Mid-Atlantic Ridge; and two iron-rich crusts from

1) the Dellwood Seamount in the Northeast Pacific and 2) the FAMOUS area. In addition, the following ferromanganese deposits, whose origins are uncertain, were studied: 1) ferromanganese coatings from the Juan de Fuca Ridge, the East Pacific Rise (EPR), and the Mid-Atlantic Ridge (MAR), which occur as ubiquitous thin coatings on exposed rocks, 2) a ferromanganese impregnated sediment from the Clarion Fracture Zone, 3) a rock composed of manganese, iron, and carbonate phases from a seamount near the EPR at 19°N and 4) two manganese nodules from the EPR and the Bauer Basin, to the east. Three Equatorial Pacific manganese nodules were analyzed to compare these highly studied ferromanganese deposits to those of more probable hydrothermal origin. Samples were analyzed for major elements Fe, Mn, Si and Al, minor elements Cu, Ni, Zn, Co and Ba, volatile elements Pb, Hg, As and Sb, and rare earth elements (REE) La, Ce, Sm, Eu, Tb, Yb and Lu. Mineralogy was determined by ultra-slow scan X-ray diffraction.

Evidence of Oceanic Hydrothermal Activity

Data from a variety of sources form the basis of a model for the formation of the hydrothermal deposits which is based on the convective cooling of the oceanic crust at spreading centers by seawater circulation. Tectonic forces and contraction upon cooling of extruded basalt create extensive faulting and fracturing along the spreading axis. Cold, dense seawater penetrates into these fractures, is heated at depth, becomes less dense, and returns to the sea floor as submarine hot springs (Elder, 1965). Heat removal by this process is much more efficient than conduction and has been used to account for both the

variability and low mean heat flow on the Juan de Fuca Ridge (Lister, 1972), the MAR (Talwani et al., 1971), and the Galapagos Spreading Center (Williams et al., 1974). Bottom water temperature anomalies, believed to indicate plumes from hydrothermal emanations, offer further evidence of this proposed system. Such temperature anomalies have been found at the Galapagos Spreading Center (Williams et al., 1974), the MAR at 26°North (Rona et al., 1974), EPR at 21°North (Crane and Normark, 1975) and recently in an area north of the Clarion Fracture Zone (H. Beiersdorf, pers. comm.).

Chemical Interactions in Hydrothermal Systems

Extensive chemical interactions between the seawater and hot rock occur during the hydrothermal process. A large body of evidence has been gathered which indicates Fe, Mn and probably other elements are leached from the basalt under reducing conditions within the rock mass. These are carried to the sea floor where they precipitate in the relatively highly oxygenated bottom water. Experimental studies of seawater-basalt interactions under heat and pressure have shown that Fe, Mn, SiO₂, H⁺ and to a lesser extent Zn, Cu and Ni are solubilized (Bischoff and Dickson, 1975; Hajash, 1975; Mottl et al., 1974; Seyfried and Bischoff, 1977). This agrees well with Corliss' (1971) observation of the depletion of Fe and other metals from the interiors of pillow basalts as compared to their relatively unaltered glassy margins.

Metalliferous accumulations on the EPR and in the Bauer Basin are considered the result of precipitation of metals from hydrothermal solutions formed at the Rise crest. Both the high metal content of

these sediments (Bostrom and Peterson, 1966; 1969) and isotopic composition of strontium and particularly lead (Dasch et al., 1971; Bender et al., 1971; Dymond et al., 1973) indicate such an origin.

Direct observations of metal rich fluids emanating from sites of shallow water submarine volcanism have been made at several locations, including the volcano Banu Wuhu in Indonesia (Zelenov, 1964), the island of Santorini in the Mediterranean Sea (Bonatti et al., 1972b), Matupi Harbor, New Britain (Ferguson and Lambert, 1972), the Solomon Islands (J. Dymond and E. J. Dasch, pers. comm.), and on the tip of the Reykjanes Peninsula on Iceland (Tomasson and Kristmannsdottir, 1972). Iron and other metal oxide precipitates cloud the water and coat the sea floor at these sites in a process believed to be similar to that occurring at active spreading centers.

Recently, the first direct observations of thick manganese and iron encrustations around fissures on the MAR were made by the French submersible Archimede during the French-American Mid-Ocean Undersea Study (FAMOUS) program. There can be little doubt that these thick crusts, and similar crusts dredged from other locations, are direct precipitates of hydrothermal solutions. They are therefore the most direct link yet found to ridge-crest hydrothermal processes, and offer an excellent way in which the composition of the fluids and the nature of the precipitation process can be examined.

Volatile Elements

The possible association of the volatile elements Hg, As, Sb and Pb with submarine hydrothermal processes is also of interest because of

their universal association with volcanic activity. Enrichments of these elements have been found in metalliferous sediments from all active oceanic ridges. Bostrom and Peterson (1969), Bostrom and Fischer (1969) and Bostrom and Valdes (1969) found Hg and As in metalliferous sediments to have their highest concentrations in areas of high heat flow. Cronan (1972) found enrichments of Hg and As in sediments from the median valley of the Mid-Atlantic Ridge, which he attributed to submarine hydrothermal activity at the ridge crest. Horowitz (1970) found Pb to be associated with active ridge process in the Pacific, Atlantic and Indian Oceans. Variations in the Hg content of manganese nodules has been related to their proximity to submarine volcanic sources (Harriss, 1968).

Geochemical budget calculations indicate that it is difficult to account for the concentrations of the volatile elements, as well as manganese, in pelagic sediments by continental weathering alone. Horn and Adams (1966) used a computer model to simultaneously calculate geochemical balances for 65 elements. Pb, As and Mn were among 10 of these elements that could not be brought into balance. Excess Sb (Onishi and Sandell, 1955b) and Hg (Goldschmidt, 1954) have been calculated by other investigators. A volcanic or hydrothermal source of these elements may account for this excess.

SAMPLES

Hydrothermal Crusts

This group of samples consists of thick crusts of probable hydrothermal origin which were dredged or collected in-situ from active oceanic spreading centers. These samples include both manganese-rich and iron-rich deposits, which are believed to represent end members of the fractionation of manganese and iron during oxidation and precipitation from hydrothermal solution (Bonatti et al., 1972c). The group consists of 1) four manganese-rich crusts from within or near the Trans-Atlantic Geotraverse (TAG) hydrothermal area, which is located at 26°N on the Mid-Atlantic Ridge (M. R. Scott et al., 1974; R. B. Scott et al., 1974; Scott et al., 1976); 2) a manganese crust from the Galapagos Spreading Center (Moore and Vogt, 1975); 3) a manganese-rich crust and an iron-rich crust, both from the FAMOUS dive site on the Mid-Atlantic Ridge; 4) an iron-rich deposit from the Dellwood seamount in the northeast Pacific (Piper et al., 1975).

Samples of special note are those from the FAMOUS area and three of the TAG samples, from just outside the hydrothermal field. The FAMOUS samples were collected by the French submersible Archimede and are among the first hydrothermal deposits observed and sampled in situ from the sea floor. The TAG samples consist of individual crusts containing two distinct layers; a thick, metallic basal layer, believed to be hydrothermal in origin, overlain by a thin and friable ferromanganese layer. These are unique samples which appear to record a change in environment as they moved away from the Mid-Atlantic Ridge

spreading axis (Scott et al., 1976).

Ferromanganese Coatings and Nodules

This group of samples consists predominantly of thin, 1 to 5 mm thick ferromanganese coatings found on pillow basalts dredged from the Juan de Fuca Ridge, the East Pacific Rise, and the Mid-Atlantic Ridge. Such deposits are common occurrences in dredge hauls, and were found by the FAMOUS dive teams to be nearly ubiquitous on exposed rock surfaces. Also studied were ferromanganese impregnated sediment from the "warm water" area near the Clarion Fracture Zone (Gundlach et al., 1976), and a deposit containing iron-rich and manganese-rich phases from a seamount at 19°S near the East Pacific Rise.

Five ferromanganese nodules from two distinct environments were studied. Three are from the Equatorial Pacific area of high productivity and have been extensively studied in the past. These were used both to check analytical procedures and to represent "normal" manganese nodule deposition. Two other nodules, one from near the East Pacific Rise crest and one from the Bauer Basin, represent nodule formation which may be influenced by ridge volcanism.

Sample descriptions are given in Appendix 1.

METHODS OF ANALYSIS

Sample Preparation

Between 200 mg and 1 gm of material was chipped or scrapped from fresh surfaces of crusts and nodules using non-metallic instruments to avoid metal contamination. Whole-crust or nodule samples were taken through the complete thickness of the crust or diameter of the nodule. The sample was ground in an agate mortar, which was cleaned between samples with $\text{HCl}_{(\text{conc})}$ and $\text{HNO}_{3(\text{conc})}$. The only exception to this sampling procedure were three of the manganese nodules, MN1641, MN1642, and MN1763, which had been sampled and ground by other researchers. Sample splits were taken for 1) flame and Carbon Rod atomic absorption spectroscopy (AAS), 2) cold-vapor AAS mercury analysis, 3) instrumental neutron activation analysis (INAA), and 4) X-ray diffraction analysis. Analyses were performed in the preceding order of preference if not enough material was available for all analyses. INAA and AAS splits were dried at 110°C for 2-3 hours just prior to analyses, to remove adsorbed water. Mercury analyzed samples were dried in a dessicator for 24 hours, instead of heating, to avoid Hg loss by volatilization.

X-ray diffraction samples were crushed to approximately 40 mesh (sand size) in the dry mortar. Subsequent grinding was done by auto-grinder under butanol, or by hand under liquid nitrogen. The liquid nitrogen technique has been used to inhibit the collapse of the frail oxide crystal structures due to oxidation during grinding (Brown, 1972). It appears that butanol also inhibits crystal collapse (M. Lyle, pers. comm.; this paper). The colors of some of the samples

became lighter after grinding under butanol, suggesting that oxidation had occurred. However, diffraction peaks of samples ground under butanol were as sharp as duplicate runs of samples ground under liquid nitrogen, suggesting that no crystal collapse results from this grinding procedure.

Atomic Absorption Spectroscopy

The elements Al, Si, Ca, Mn, Fe, Ni, Cu, Zn, Ba, Hg and Pb were analyzed by AAS after total acid digestion in Teflon-lined bombs. A Jarrell-Ash Model 810 Spectrophotometer was used for analysis of all elements except Hg. A special cold-vapor technique, which is discussed in detail in the next section, was used for Hg analysis. For the elements besides Hg, 100 to 150 mg samples were dissolved in Teflon-lined bombs containing 2 ml aqua regia and 6 ml HF. The bombs were heated at 110° C for two hours. After cooling, excess HF was neutralized by the addition of 5.6 gm H₃BO₃, and the samples were diluted to the desired concentration range. Standards were prepared in the same HF-aqua regia-H₃BO₃ matrix from either commercial standard solutions or by dissolution of pure metals (or SiO₂ in the case of Si) in either HCl (Fe, Mn, Cu, Ni, Zn and Ca), aqua regia (Al and Ba), or aqua regia and HF (SiO₂).

Conventional flame absorption was used for all elements except Pb, which required greater sensitivity than was possible with a flame. Flameless analysis was performed utilizing a Varian Techtron model 63 Carbon Rod Atomizer (CRA). This technique employs a graphite electrode which holds a single aliquot of sample solution. A three step cycle

of progressive temperature increases vaporizes the matrix components before final atomization, thus eliminating most interferences. Table 1 lists the operating parameters used for the analyses.

Cold Vapor AAS of Mercury

Because of the extremely low levels of Hg in ferromanganese deposits (Harriss, 1968), a very sensitive technique of analysis, effective in the parts per billion range, is necessary. For this reason, the cold vapor atomic absorption technique was chosen. It involves the chemical reduction of Hg(II) ions in solution to neutral Hg atoms by a suitable reducing agent. The sample is then aerated with a carrier gas which carries the Hg atoms into a cell where absorbance is measured at 254 nm.

For all analyses, a recently designed instrument was used which maximizes sensitivity by using a small volume reduction vessel, rapid aeration and long absorption cell (Hawley and Ingle, 1975; Christmann and Ingle, 1976). The reduction vessel is made from a 10 mm diameter glass tube fitted with a porous glass frit near its base. Aeration is from below, up through the glass frit and the solution. Sample volume is only 1 ml, and is injected into the reduction vessel after addition of 0.1 ml of 1% SnCl₂ reduction solution. A large effective surface area is created by the intense bubbling of the small volume of sample solution. This causes rapid diffusion of reduced Hg out of solution, enabling a very sharp absorption peak to be observed. A detection limit is therefore possible of 2×10^{-12} gm Hg (2 ppt in solution).

Table 1. Instrument Parameters for Atomic Absorption Spectroscopy

Element	Wave length	Slit Width	Lamp Current	Oxidant/ Fuel	Comments
Al	3093Å	4Å	10 ma	N ₂ O ₂ /C ₂ H ₂	
Ba	5536	2	15	N ₂ O ₂ /C ₂ H ₂	
Ca	4227	10	10	N ₂ O ₂ /C ₂ H ₂	
Cu	3247	4	7	Air/C ₂ H ₂	
Fe	2483	2	8	Air/C ₂ H ₂	
Mn	2795	4	10	Air/C ₂ H ₂	
Ni	2320	1	10	Air/C ₂ H ₂	Bkgd. 2316Å
Si	2516	2	12	N ₂ O ₂ /C ₂ H ₂	
Zn	2139	10	7.5	Air/C ₂ H ₂	Bkgd. 2100Å
Pb	2833	4	5	CRA	Bkgd. 2820Å

CRA (Pb)

Dry: 2.5V/35 sec.

Ash: 4.5V/12 sec.

Atomize: 9V/3.5 sec.

H₂ Flow: 1

Fifty mg samples were digested in Teflon-lined bombs using 2 ml HF purified by low-temperature distillation (Mattinson, 1972), and 0.3 ml $\text{HNO}_3(\text{conc})$ (reagent grade). After heating for 2 hours and cooling, 1.9 gm H_3BO_3 was added directly into the Teflon liner. The solution was brought to a final volume of 25 ml and immediately analyzed. The Hg concentration in this solution was usually 0.1 to 5 ppb. Standards were prepared from a Hg (II) stock solution and contained 5% HNO_3 (v/v) and 0.01% $\text{K}_2\text{Cr}_2\text{O}_7$ (w/v) as a preservative (Christmann and Ingle, 1976). The addition of the acids used in sample digestion to standard solutions had no detectable effect on the Hg peaks obtained, indicating that matrix effects are minimal. This was confirmed by adding known amounts of Hg to digested samples and comparing with standard solutions. Blanks were determined by taking reagents only through the digestion procedure with each group of samples analyzed.

Hg contamination was found to be a significant problem at these low levels. To minimize this, glassware was prepared by cleaning with a dilute KMnO_4 - HNO_3 solution overnight, and rinsing with $\text{HCl}(\text{conc})$ and $\text{HNO}_3(\text{conc})$ before each use (Hawley and Ingle, 1975; Christmann and Ingle, 1976). Teflon liners were cleaned periodically by twice heating overnight with them containing 2 ml distilled $\text{HF}(\text{conc})$ and 0.5 ml HNO_3 . This procedure effectively leaches Hg from within the porous Teflon (R. Senechall, pers. comm.). The liners were also cleaned after each analysis by boiling in $\text{HNO}_3(\text{conc})$ for one hour.

All chemicals used were reagent grade except hydrofluoric acid, which was found to be the major source of Hg blank. Low temperature distillation of reagent grade HF was found to reduce its Hg content

from 1 ppb to 0.6 ppb. Hg concentrations in the final, diluted blank solutions were 0.06 to 0.08 ppb.

The precision of this analytical procedure has been determined by multiple analysis of each sample. The relative standard deviation for repeated total analysis, including digestion, of individual samples is 5-10% for samples with greater than 300 ppb Hg, 10-20% for samples with Hg concentrations in the 50-300 ppb range, and 30-60% for those with less than 50 ppb.

An indication of the accuracy of these analyses has been obtained by analysis of U.S.G.S. standard rock GSP-1. The mean value obtained falls within the range of values found by other investigators (U.S.G.S., 1970), but above their mean value (see Table III-1).

Instrumental Neutron Activation Analysis

As, Sb, Co, and the rare earth elements La, Ce, Sm, Eu, Tb, Yb and Lu were analyzed by INAA. Between 150 and 200 mg samples were irradiated in the rotating rack of the Oregon State University TRIGA reactor for from 3 to 6 megawatt hours. Counting was done with a Ge(Li) detector coupled to either a 2048 or a 4096 channel Nuclear Data multi-channel analyzer. Errors were calculated on the basis of counting statistics, or results of duplicate analysis, when possible. Two sets of counts were made for each sample: 1) after 6-7 days decay time, for elements with half-lives less than 5 days, and 2) after 3-4 weeks, for elements with half-lives greater than 5 days. Concentrations were calculated by comparison with As, Sb and rare earth element liquid standards, U.S.G.S. rock standards CRB-1 and GSP-1, manganese

nodule standard GRLD-126 and O.S.U. metalliferous sediment standard MS-1519, all of which were irradiated and counted with the samples.

X-ray Diffraction Analysis

Mineralogy was determined by ultra-slow scan X-ray diffraction, using Cu irradiation. Random mounts of ground material were scanned from 5 to 70 degrees 2θ at a rate of 500 seconds per degree. Data was digitally recorded, and noise and background were removed by numerical methods similar to those of Dasch et al. (1971).

MINERALOGY

The X-ray diffractograms of the samples show that most of them contain one dominant mineral. For the Mn hydrothermal crusts this mineral is birnessite, identified by its strong 7 \AA and 3.6 \AA , and weak 2.4 \AA and 1.42 \AA peaks (Burns and Burns, 1977), or todorokite, with its strong 9.8 \AA and weak 2.4 \AA and 1.42 \AA reflections (Burns and Burns, 1977). Very highly crystalline birnessite was found in all samples of the Galapagos Spreading Center and TAG hydrothermal crusts that were analyzed. This X-ray data confirms the SEM identification of bladed birnessite crystals in other TAG hydrothermal samples (Scott et al., 1976). Todorokite, and minor birnessite peaks dominate the FAMOUS Mn-rich deposit (MN1776) diffractogram.

Diffractograms of the ferromanganese coatings exhibit weak reflections at 2.4 \AA and 1.42 \AA only (plus some accessory mineral peaks), indicative of δMnO_2 (Burns and Burns, 1977). Very weak, broad reflections at 7 \AA are also present in these samples. These reflections probably result from phillipsite and the 002 reflection of a poorly crystalline smectite, since the lack of a 3.6 \AA peak indicates birnessite is not present.

The EPR nodule MN1468 was the only nodule analyzed by X-ray diffraction in this study. Its diffraction patterns is similar to those of the ferromanganese coatings, with δMnO_2 the only identifiable manganese mineral.

According to Lyle et al. (1977), the Bauer Basin nodule (MN1188) consists primarily of todorokite with minor amounts of δMnO_2 . The

Pacific nodules (MN1641 and MN1642) are primarily birnessite (Piper, 1974).

The three Fe-rich crusts, including the iron-rich AMPH D6 phase, have diffraction patterns which indicate that most of the Fe is in amorphous or smectite phases. The Dellwood Seamount crust (MN1775) gives no significant diffractions at all and can be considered truly amorphous. A small amount of goethite is identifiable in the pattern of the AMPH D6 iron phase (MN1727), but this sample appears to be mostly amorphous. The FAMOUS iron-rich crust (MN1777) gives a strong smectite pattern indicative of a nontronite-montmorillonite. Weak birnessite peaks are also present, indicating the small admixture of manganese material in this sample.

The accessory minerals identifiable in the ferromanganese coatings and nodules are quartz, phillipsite, calcite, and possibly smectite. Quartz and phillipsite peaks are present in all of these sample's diffractograms. Calcite is found in only one sample (MN1657) and smectite peaks are weakly evident for one crust (MN1660) and questionable for a few others. The hydrothermal crust patterns show no extraneous peaks besides those of the manganese or iron minerals already discussed.

The mineralogy of these samples are summarized in Table 2.

TABLE 2. Mineralogy Results from X-ray Diffraction Analyses.

Sample Type	Sample No.	Mn or Fe Mineral Present	Accessory Mins.
Hydrothermal Crust	MN1749	B	--
	MN1896	B >> T	--
	MN1846	B ¹	--
	MN1848	B ¹	--
	MN1850	B ¹	--
	MN1750	B	--
	MN1751	B	--
	MN1752	B	--
	MN1776	T >> B	--
	MN1777	Sm	--
	MN1775	Amorph.	--
	MN1728	Amorph.-Goeth?	--
Ferromanganese Coatings	MN1659	δ MnO ₂	Phil., Qtz.
	MN1626	δ MnO ₂	Qtz., Phil., Sm?
	MN1660	δ MnO ₂	Sm?
	MN1627	δ MnO ₂	Qtz., Phil.
	MN1630	δ MnO ₂	Qtz., Phil.
	MN1657	δ MnO ₂	Calcite
	MN1194	δ MnO ₂	Phil.
	MN1768	δ MnO ₂	Phil.
	MN1628	δ MnO ₂	Qtz., Goeth.
	MN1629	δ MnO ₂	Qtz., Phil., Goeth.
Manganese Nodules	MN1468	δ MnO ₂	--
	MN1188	T >> δ MnO ₂ ²	--
	MN1641	B ³	--
	MN1642	B ³	--
	MN1763	--	--

B = birnessite
T = todorokite
Sm = smectite
Phil = phillipsite

¹ Scott et al. (1976)

² Lyle et al. (1977)

³ Piper (1974)

CHEMISTRY RESULTS

Major and Minor Elements

The results of major and minor element analysis (Table II-1) show several distinctions between the hydrothermal crusts, ferromanganese coatings and nodules. Figure 1-3 illustrate two major distinctions, 1) enrichment of minor element contents in the sequence hydrothermal crusts < ferromanganese coatings < manganese nodules, and 2) enrichment of iron and silica in the sequence nodules < ferromanganese coatings < hydrothermal iron crusts. Also shown in Figures 1 and 2 is the similarity in composition between ferromanganese coatings and metalliferous sediment from the EPR.

The ternary diagram of Fe vs. Mn vs. (Co + Ni + Cu) (Figure 1) depicts the fields of "hydrothermal" and "hydrogenous" deposition of Bonatti et al. (1972c) and also shows a third field defined by the chemistry of the ferromanganese coatings of this study. This field lies on a tie line between the Fe end member and the nodule field, thus demonstrating both the enrichment of iron and depletion of trace metals in the ferromanganese coatings as compared to nodules. Average Fe/Mn ratios of 2.2 for coatings versus 1.1 for nodules also demonstrate the iron enrichment in ferromanganese coatings. Bulk analysis of metalliferous sediment from the EPR and authigenic smectite from the Bauer Deep have also been plotted in Figure 1. They can be seen to occupy the same fields as the ferromanganese coatings and iron-rich hydrothermal crusts respectively.

A few of the samples have compositions that are anomalous. The

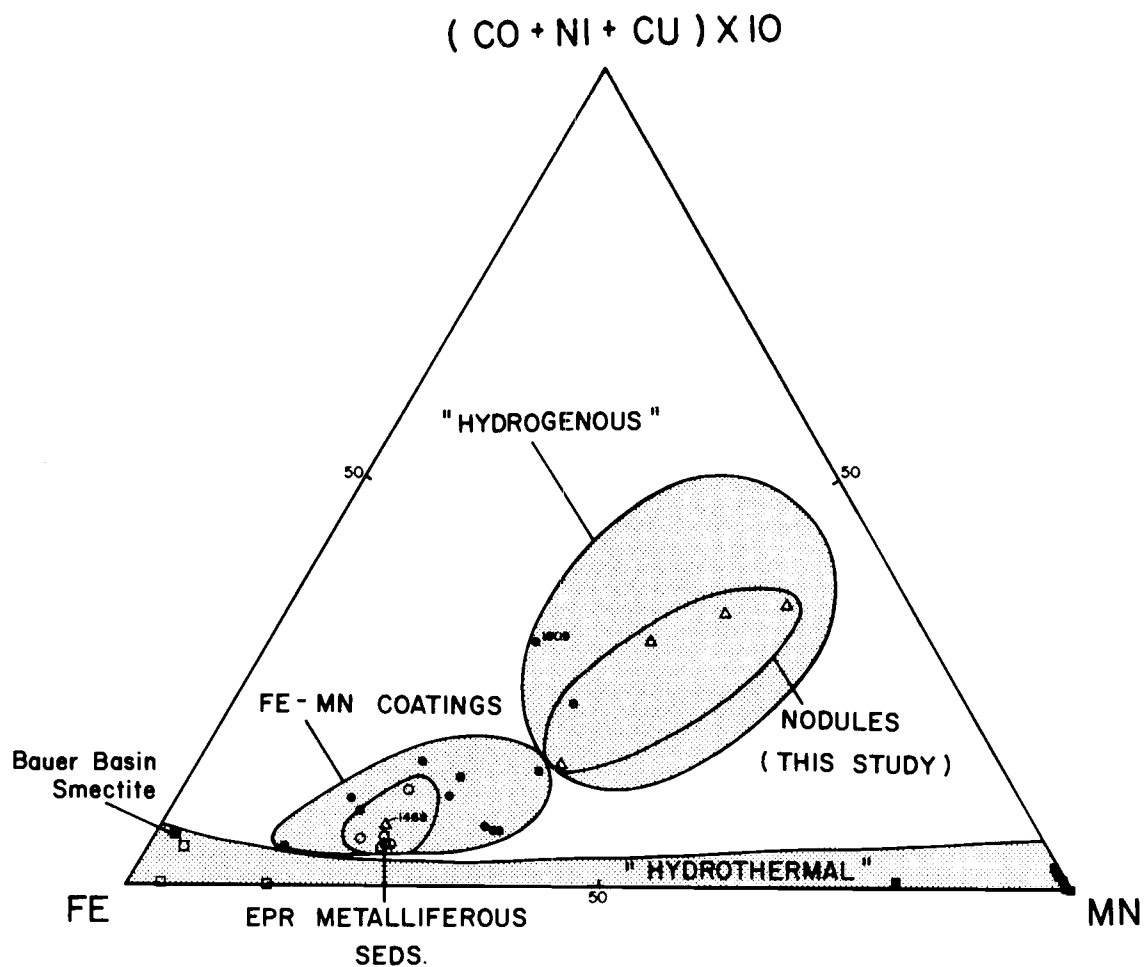


Figure 1. Ternary diagram of Fe vs. Mn vs. Co + Ni + Cu, showing 1) the low trace metal content of hydrothermal crusts, and 2) the enrichment of Fe and depletion of trace metals in ferromanganese coatings and EPR metalliferous sediments relative to manganese nodules. "Hydrogenous" and "Hydrothermal" fields are from Bonatti et al., 1972c. EPR metalliferous sediment data is from Corliss and Dymond, 1975. Bauer Basin smectite data is from Eklund, 1974.

EPR nodule (MN1468) has a composition similar to ferromanganese coatings and metalliferous sediments rather than nodules. The ferromanganese impregnated sediment (MN1809, MN1810, MN1811) has a somewhat unique composition, falling outside the ranges of both ferromanganese coatings and nodules. The AMPH D6 sample is highly unusual, in that the manganese-rich phase (MN1727) is similar to ferromanganese coatings, but the iron-rich phase is identical to the iron-rich hydrothermal crusts.

Si enrichments are found to correspond to those of Fe in the ferromanganese coatings, metalliferous sediments and iron hydrothermal crusts. A nearly linear increase of Si with Fe is shown in the ternary diagram of Fe vs. Mn vs. Si (Figure 2). The strong correlation of these two elements may indicate that they have a common source in ferromanganese coatings and hydrothermal crusts. The samples that are anomalous in Figure 1 again stand out in this plot. The high Si contents of the ferromanganese impregnated sediment samples are due to the large amount of Si in the clay they contain. The EPR nodule (MN1468) again plots within the ferromanganese coating field. The AMPH D6 manganese phase (MN1727) is unlike any of the groups.

The origin of the Si in some of these samples may be deduced by comparing their Si versus Al concentrations. Many of the nodules, as well as the impregnated sediment, have Si/Al ratios of approximately three, suggesting that Si is in the form of detrital grains that have been incorporated into the deposits (average Si/Al ratio for marine sediments = 3 (Turekian and Wedepohl, 1961)). The ferromanganese coatings have a mean Si/Al ratio of 5.1, indicating that there is an

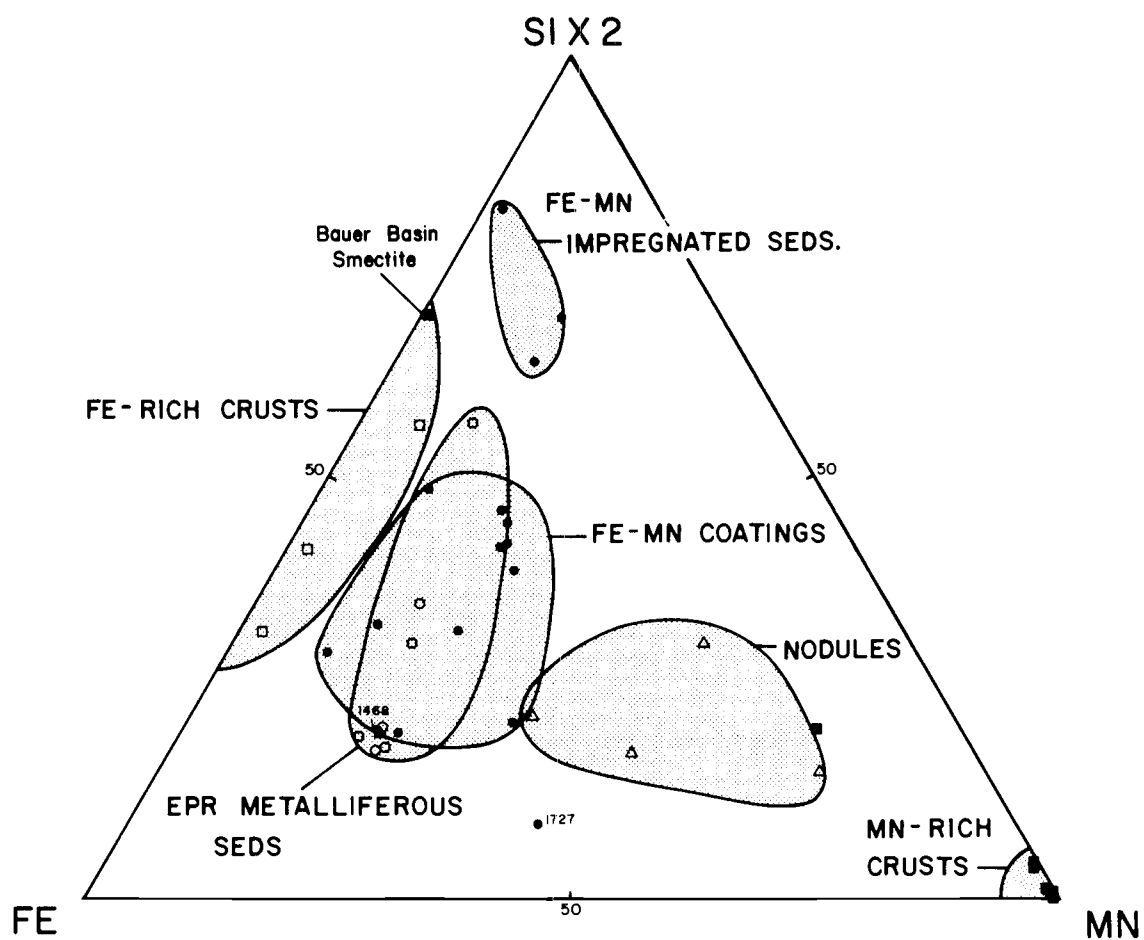


Figure 2. Ternary diagram of Fe vs. Mn vs. Si showing the correlation of Fe and Si in these samples. EPR metalliferous sediment data is from Corliss and Dymond, 1975. Bauer Basin smectite data is from Eklund, 1974.

additional source of Si in these deposits. High Si contents, combined with extremely low Al concentrations (<200 ppm) give the iron-rich hydrothermal crusts extraordinarily high Si/Al values of 600-900. High Si/Al ratios, of 10-20, are also found in some of the hydrothermal manganese-rich crusts. The absolute values in these samples are so low, however, that analytical errors make the Si/Al values uncertain. Si vs. Al concentrations are plotted in Figure 3.

A microscopic examination of the hydrothermal crusts revealed that Si is not in the form of biogenic opal, but appears to exist as clay aggregates (smectite) in MN1777 and as orange-brown, very fine grained translucent material in MN1775. Biogenic calcite, in the form of foraminifera, are present in the ferromanganese coatings, so it may be assumed that some biogenic opal is also present. None of these crusts, however, are from areas of high primary productivity, and it is unlikely that all of the excess Si they contain is biogenic in origin. The excess Si may instead be silica precipitated from hydrothermal sources.

The Fe/Si value of the FAMOUS iron-rich smectite (MN1777) is 1.3, equal to that of a smectite in which iron has substituted into all octahedral and available tetrahedral sites. All the iron and silica in this sample can therefore be accounted for by this smectite phase. The amorphous iron-rich crusts (MN1728 and MN1775) contain considerably less silica, relative to iron, than is necessary for the formation of smectite.

Significant variations in the relative concentrations of the trace metals Co, Ni, Cu and Zn have been found for the different types

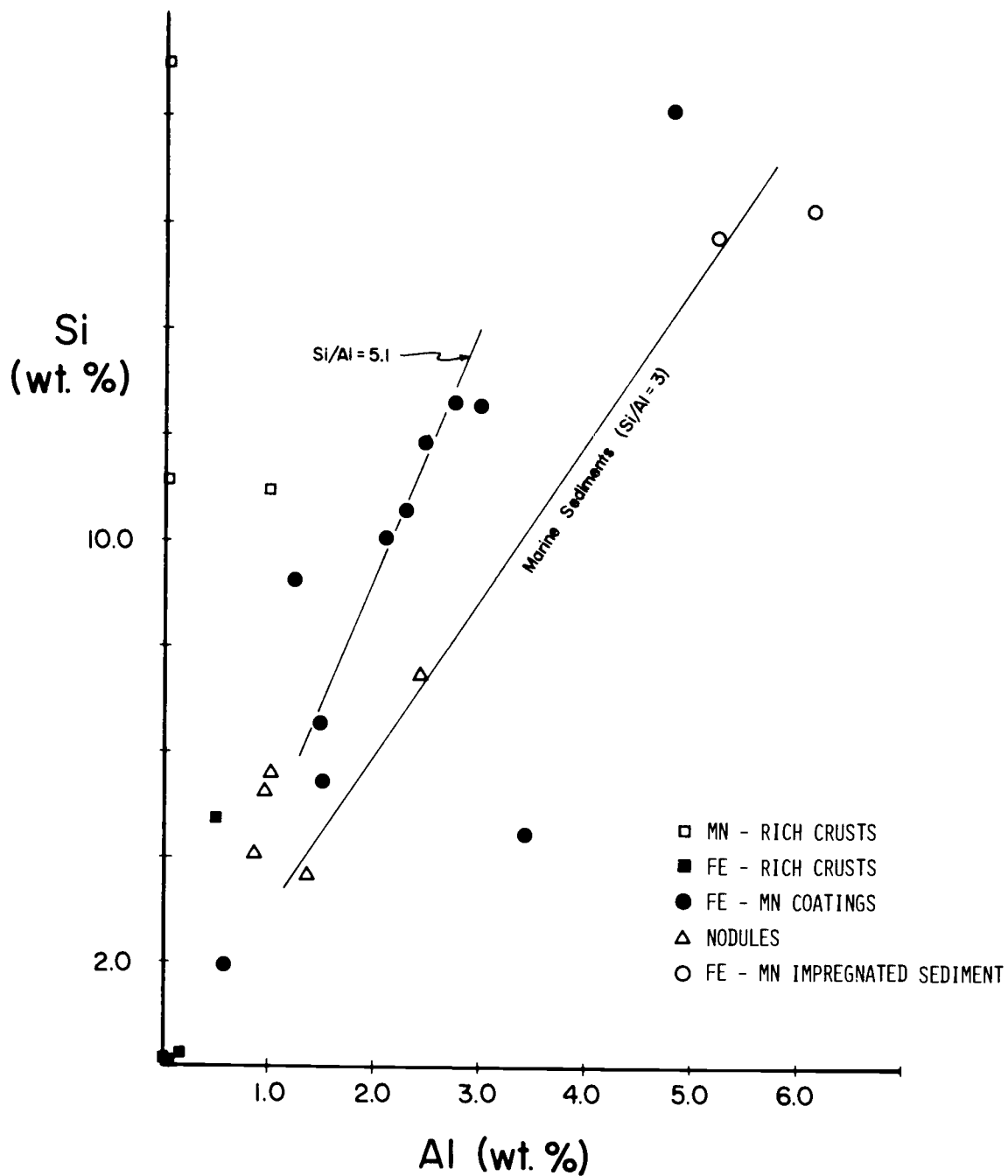


Figure 3. Si vs. Al concentrations. Si/Al ratios of nodules are shown to be similar to marine sediments. Ferromanganese coatings and Fe-rich crusts show enrichments in Si. Average marine sediment value is from Turekian and Wedepohl, 1961.

of samples of this study. Comparisons of the various elemental ratios indicate that Zn is enriched relative to the other metals in hydrothermal crusts, while Co is enriched in ferromanganese nodules and coatings. These enrichments are illustrated in the ternary diagrams of Cu vs. Ni vs. Zn and Cu vs. Ni vs. Co (Figure 4). The manganese nodules and ferromanganese coatings are very similar in the relative abundances of these trace metals, occupying nearly the same regions in both diagrams. Their compositions are characterized by limited ranges of Zn and Cu, and wide ranges of Co and Ni concentrations. The iron and manganese-rich crusts are also similar to each other, with both containing relative enrichments in Zn and depletions in Co as compared to the ferromanganese nodules and coatings.

Barium concentrations correlate roughly with the abundance of trace metals. Hydrothermal crusts have very low values, nodules have the highest values, and those of ferromanganese coatings lie between the two. This correlation is illustrated by the similarity of the ternary plot of Fe vs. Mn vs. Ba (Figure 5) to Figure 1. An exception is the ferromanganese impregnated sediment (MN1809), which is high in trace metals, but has one of the lowest barium concentrations. It has been suggested that barium is an element introduced into the ocean by hydrothermal activity and concentrated in manganese-rich hydrothermal crusts (Bonatti et al., 1972a; Bonatti, 1975). Although there is a slight enrichment of barium in some of the hydrothermal crusts, this study does not corroborate Bonatti's thesis. Alternately, the high Ba contents that have been found in some deposits of probable hydrothermal origin (e.g. Nazca Plate metalliferous sediments) may result from

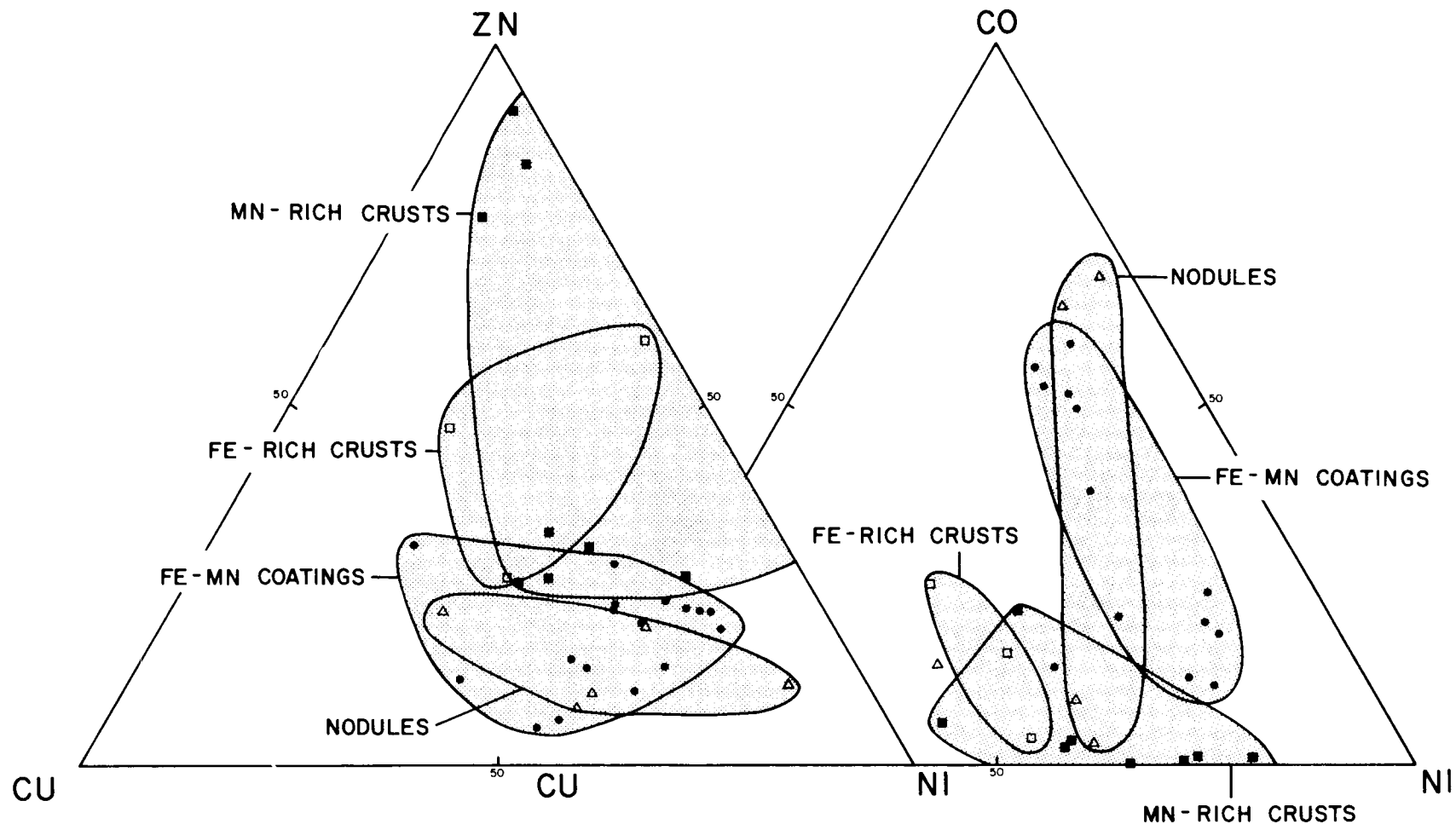


Figure 4. Ternary diagrams of Ni vs. Cu vs. Zn and Ni vs. Cu vs. Co showing relative enrichment of Zn and depletion of Co in hydrothermal crusts versus ferromanganese coatings and nodules.

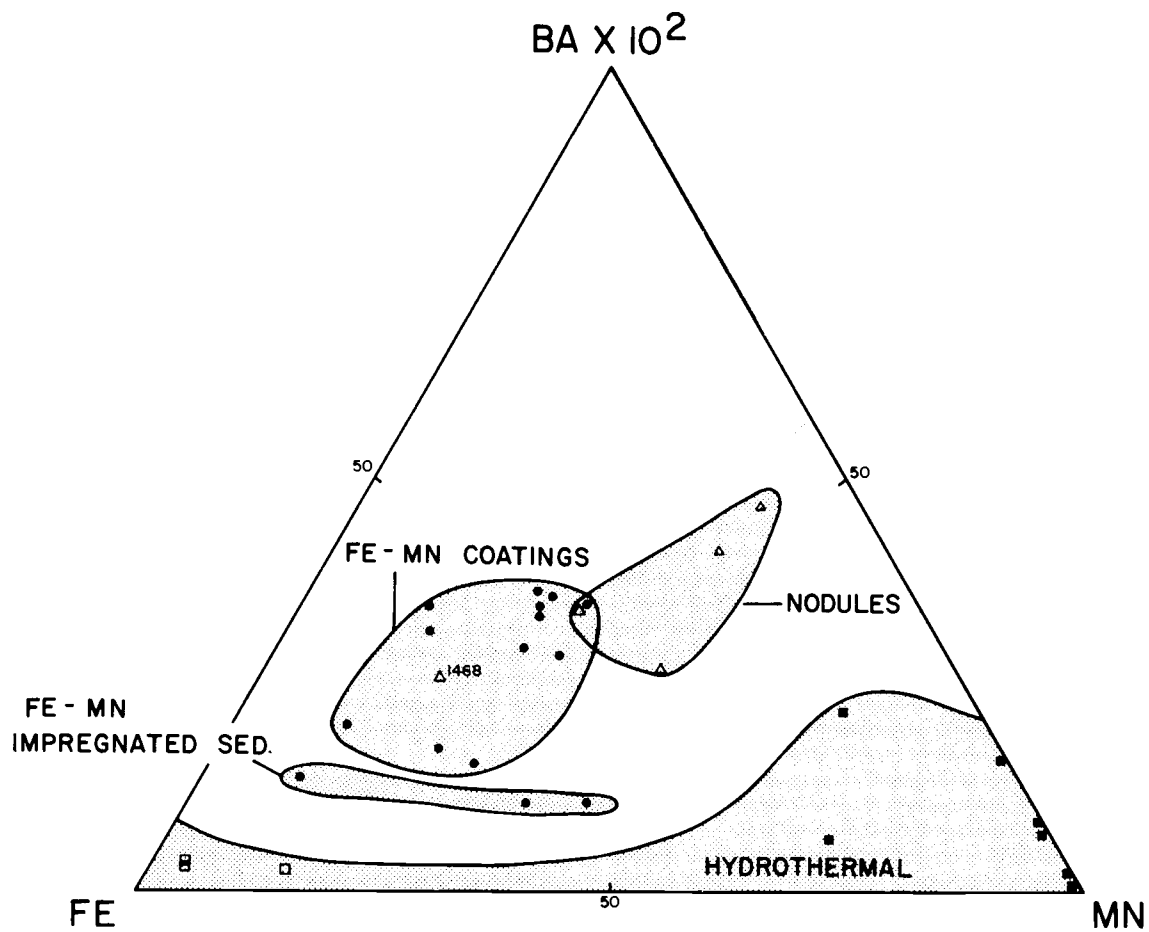


Figure 5. Ternary diagram of Fe vs. Mn vs. Ba showing the similarity in pattern of Ba concentrations to that of trace metals.

biogenic sources (Heath and Dymond, 1977).

The chemical distinctions between the different types of deposits have been summarized using the statistical process of Q-mode factor analysis (Klovan and Imbrie, 1971). Factor analysis describes most of the variance in a complex set of data in terms of a small number of statistically independent linear combinations of the original variables, known as factors. This technique had been applied to geologic problems for several years (for example, Imbrie and van Andel, 1964; Imbrie and Kipp, 1970). In this case, the raw data matrix consisted of 28 samples with 11 element variables (Al, Si, Ca, Mn, Fe, Co, Ni, Cu, Zn, Ba and Pb). Since each element is of roughly equal geochemical interest, their concentrations were normalized to give each element an equal mean value. This process preserves all of the relative relations within and among elements but avoids the dominance of factors by the most abundant elements.

Three factors were determined which account for 95% of the variance in the normalized data set. The factor loadings (relative contribution of each element) and composition of each sample in terms of these factors are shown in Figure 6. Factor 1 consists primarily of Si and Fe, and secondarily Al and Ca. It appears to represent a hydrothermal iron and silica end member. Iron-rich hydrothermal crusts show extremely high loadings in this factor. The occurrence of minor loadings of Al in this factor may reflect the presence of Al in detrital clay contained in some of the samples. Factor 2 is the Mn hydrothermal end member with secondary loadings of Al and Ca. Not surprisingly, the hydrothermal manganese crusts consist almost entirely

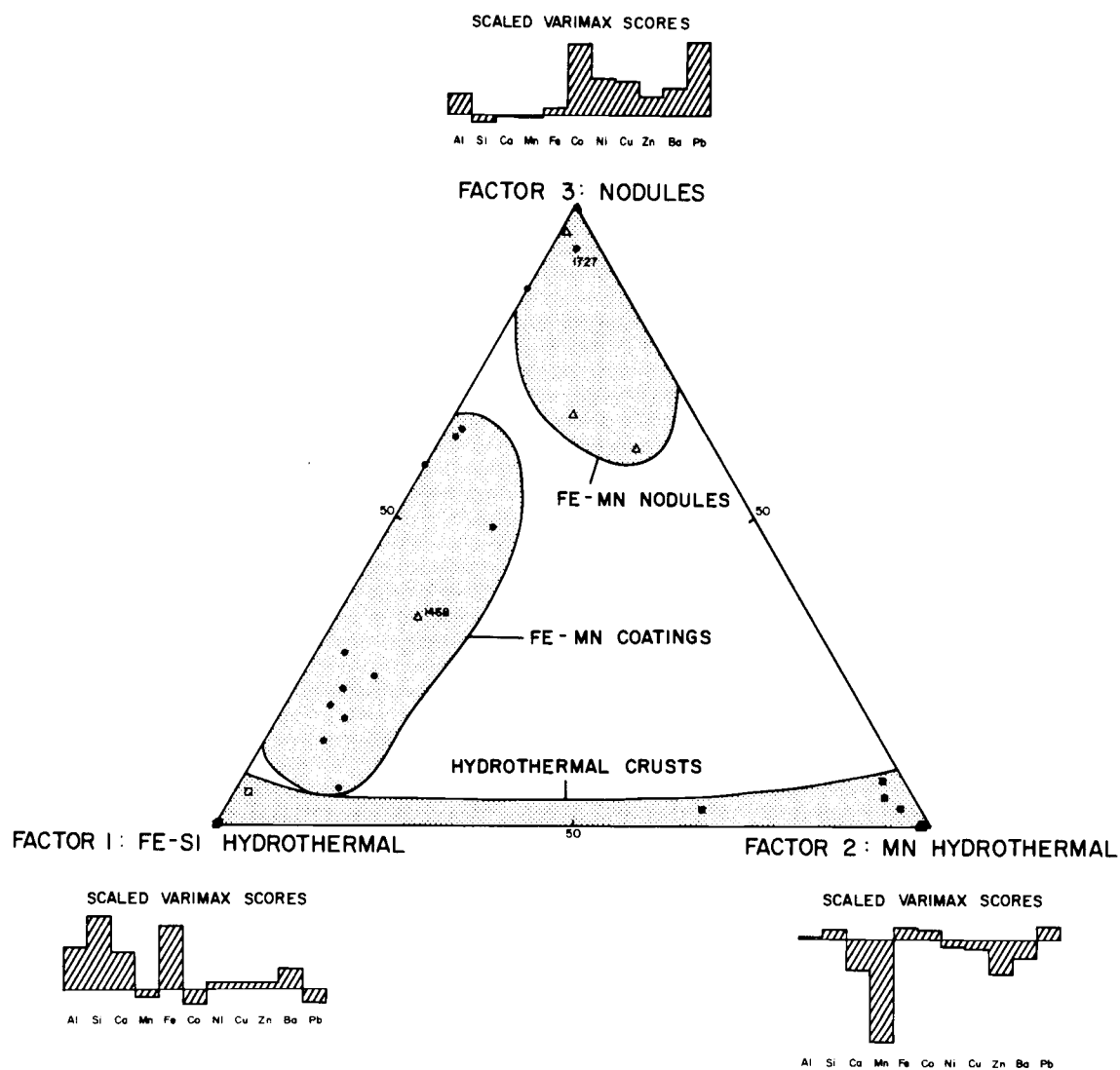


Figure 6. Ternary diagram of factor analysis results showing elemental loadings of each factor and relative abundance of factors in each sample.

of this factor. Factor 3 consists primarily of Pb, Co, Ni, and Cu, and appears to represent a nodule end member, since nodules have the highest loadings in this factor. As in Figures 1, 2, and 5, ferromanganese coatings have compositions transitional between the iron-rich hydrothermal crusts and nodules.

The anomalous samples found in other plots, the EPR nodule (MN1468) and the AMPH D6 manganese phase (MN1727) again appear in Figure 6. MN1468 plots, as before, within the ferromanganese coating field. MN1727 is found within the field of manganese nodules.

Rare Earth Elements

The rare earth elements (REE) are a series of 14 elements whose chemical properties are similar, but whose behavior varies systematically throughout the series. The variation is caused by the gradual contraction of ionic radius along the series, owing to the increasing nuclear charge, but poor shielding of this charge by the increasing number of electrons which populate the interior 4f electron shell (Cotton and Wilkinson, 1972).

Because of the special nuclear stability of the even numbered atomic elements, there are striking differences in the abundances of successive elements with odd and even numbers in all cosmic and terrestrial matter. The usual technique of smoothing out this odd-even effect by normalizing to some standard on an element-by-element basis has been employed in this study. The standard chosen is an unweighted average of REE concentrations of shales from North America (Haskin and Haskin, 1966). The shale REE pattern more closely

approximates that of manganese nodules and other marine phases than the traditionally-used chondrite (meteorite) standard, thus allowing better comparison of small but significant differences in these samples (Piper, 1974). The REE patterns obtained are shown in Figures 7-10. The absolute concentrations of these elements are given in Table II-1.

For comparison, the shale-normalized patterns of the potential sources of REE in these deposits, seawater, tholeiites and marine sediments, are shown in Figure 11.

Most of the patterns obtained, with the exception of Ce, whose anomalous behavior is discussed below, are similar to marine sediments (relatively flat) or seawater (slightly enriched in heavy REE). Small differences found in the patterns of ferromanganese coatings and nodules (Figure 7) from different locations do not follow the trends with depth found by Piper (1974), but seem to be characteristic of local supplies of REE. The patterns of ferromanganese coatings from a single location are identical within the precision of analysis.

The hydrothermal crusts have extremely low absolute REE concentrations (1 to 2 orders of magnitude < ferromanganese nodules and crusts). Their patterns are similar to seawater, with the exception of striking Sm and Lu anomalies in some samples (Figure 8). It is possible that the anomalies are the result of analytical uncertainties at the low concentrations being measured. The anomalies, however, are much greater than the estimated analytical errors (error bars, Figure 8), which are based on counting statistics and the results of duplicate analyses. The close similarity in patterns of samples from a given location offers further evidence that these anomalies are real.

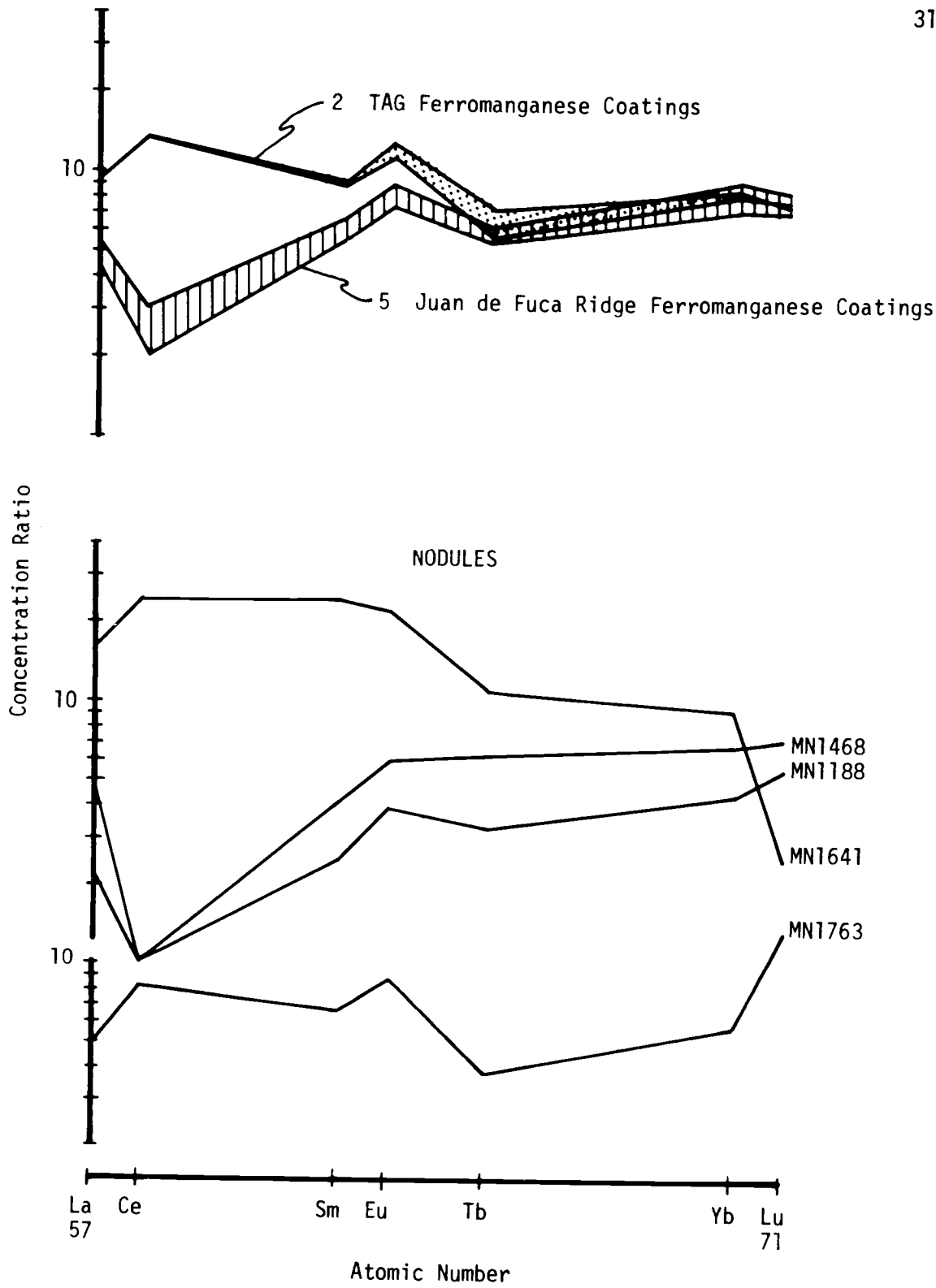


Figure 7. Shale normalized REE patterns of ferromanganese coatings and nodules showing the similarity of patterns in samples from a given location, and relative Ce enrichments in most nodules and some ferromanganese crusts.

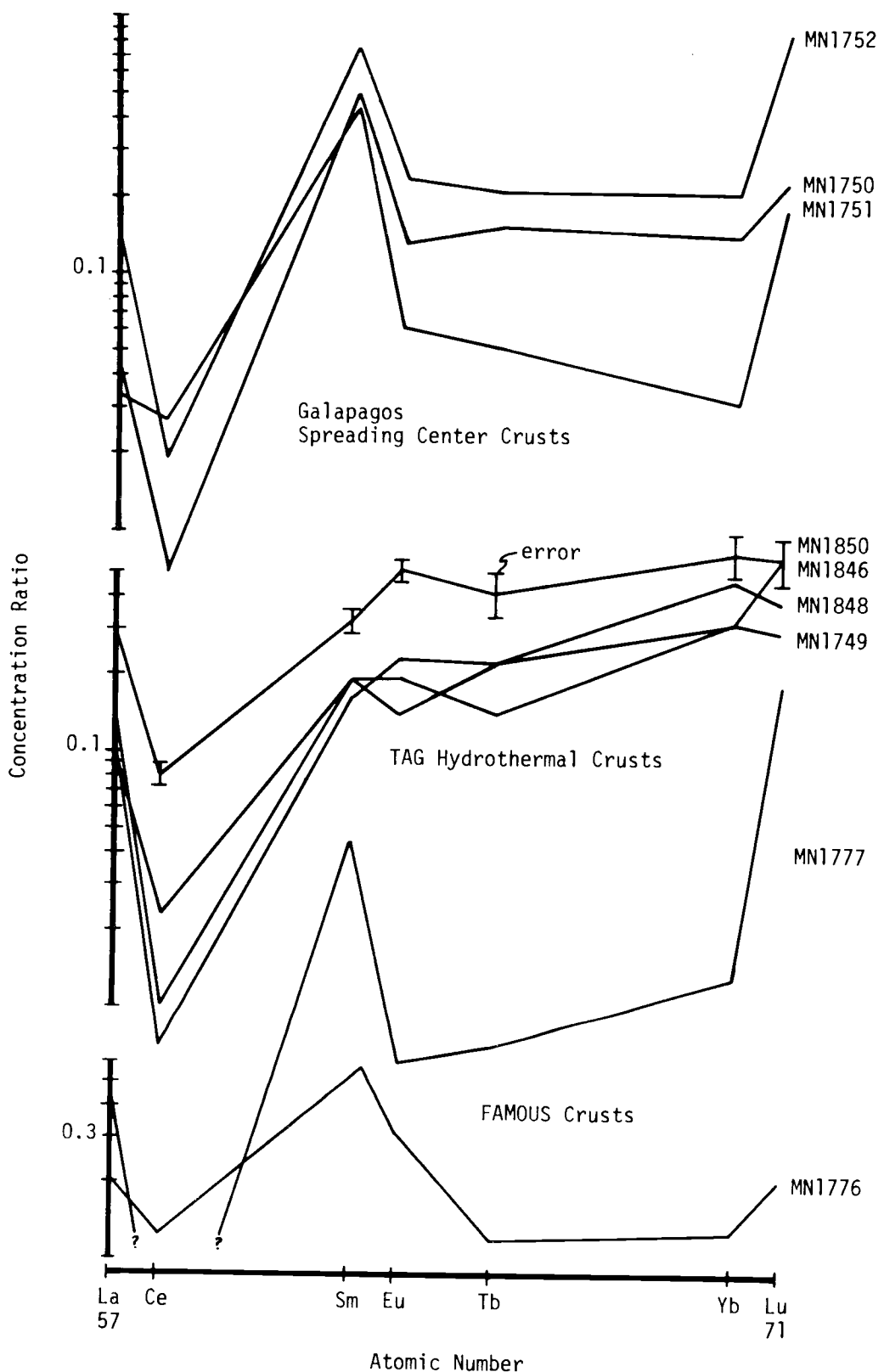


Figure 8. Shale normalized REE patterns of hydrothermal crusts showing their similarity to seawater patterns, but with striking Sm and Lu anomalies in some samples.

The REE pattern of the TAG hydrothermal crusts appears to be similar to that of seawater. Normalization of their values to the seawater average of Hogdahl et al (1968) confirms this similarity (Figure 9), and indicates that normal seawater is the lone source of REE in these deposits.

Erratic REE patterns have been found for the two AMPH D6 phases (MN1727 and MN1728) and the ferromanganese impregnated sediment (MN1809) (Figure 10). These samples have high absolute concentrations similar to ferromanganese nodules and coatings, which suggests that analytical uncertainty is not the cause of these irregularities. The nearly mirror image patterns of the two AMPH D6 samples suggests that REE were strongly fractionated during the deposition of these two phases.

Cerium is the one element in the rare earth series that exhibits anomalous behavior in the marine environment. It is highly depleted, relative to the adjacent REE, in seawater (Hogdahl et al., 1968), yet is enriched in most manganese nodules (Goldberg et al., 1968; Ehrlich, 1968; Piper, 1974). It has been suggested that both the enrichment in nodules and depletion in seawater result from the preferential incorporation of Ce from seawater into manganese nodules (Goldberg et al., 1963). Although the mechanism of Ce enrichment is uncertain, it may be related to the proposed existence of the highly insoluble Ce^{+4} ion in seawater (Goldberg, 1961).

Anomalous Ce values, as compared to Lu and Sm, have been found in nearly all the samples of this study. This cerium "anomaly" can be quantified somewhat by calculating the ratio of the measured Ce value

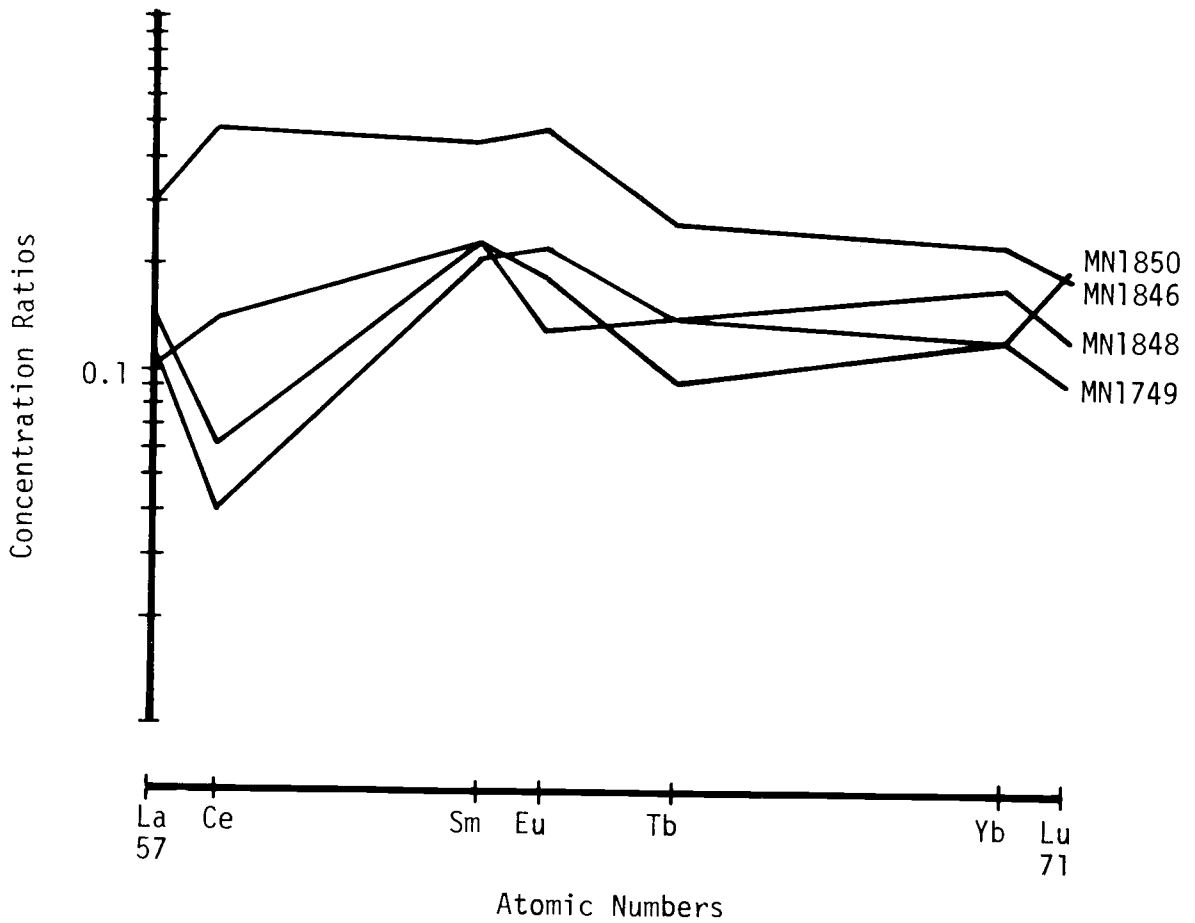


Figure 9. Seawater normalized REE patterns of TAG hydrothermal crusts showing similarity of REE to seawater throughout the rare-earth series.

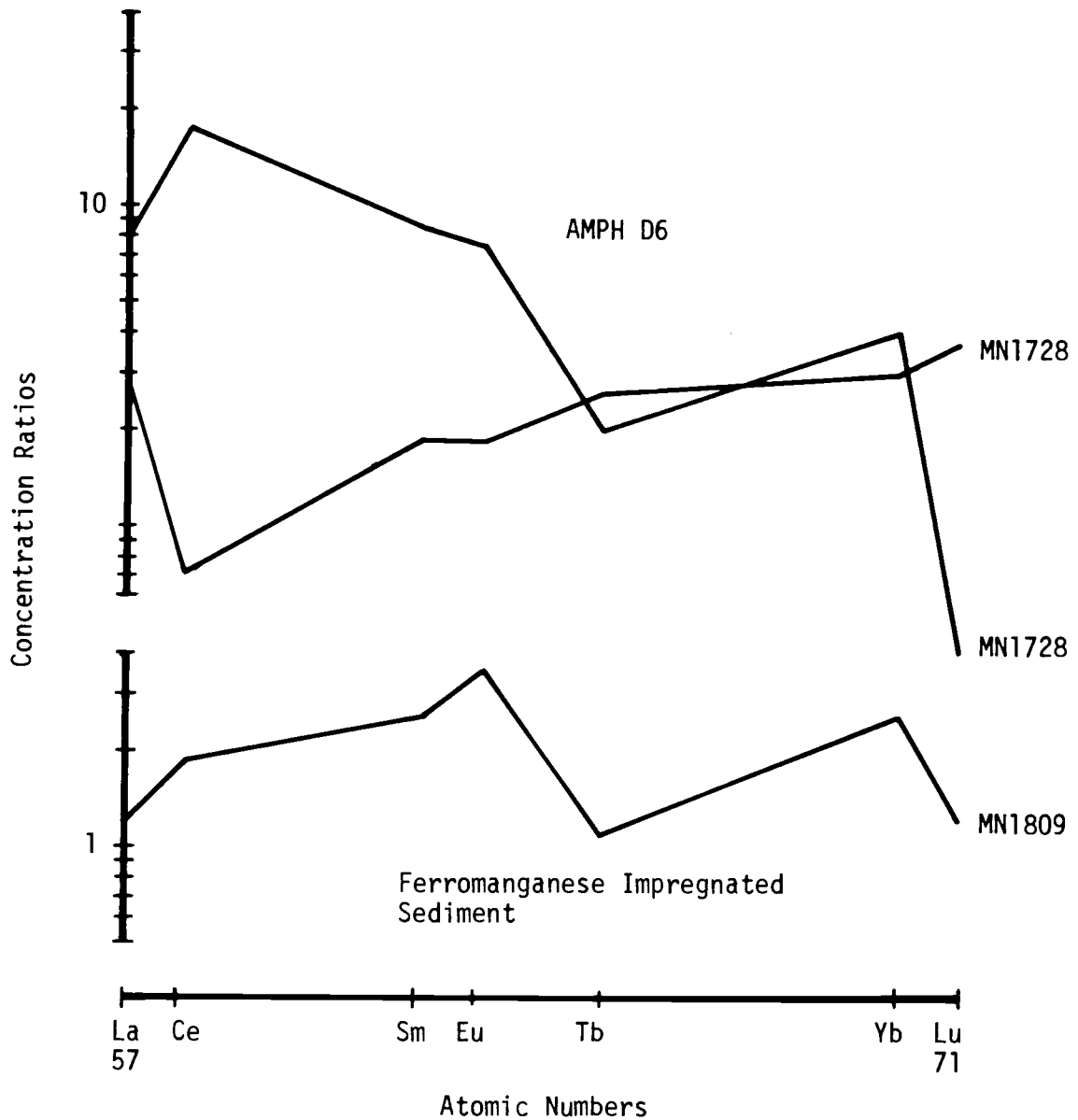


Figure 10. Shale normalized REE patterns of AMPH D6 deposits and Fe-Mn impregnated sediment showing the erratic concentrations of REE in these deposits, and possible fractionation of REE into the Fe-rich and Mn-rich AMPH D6 phases.

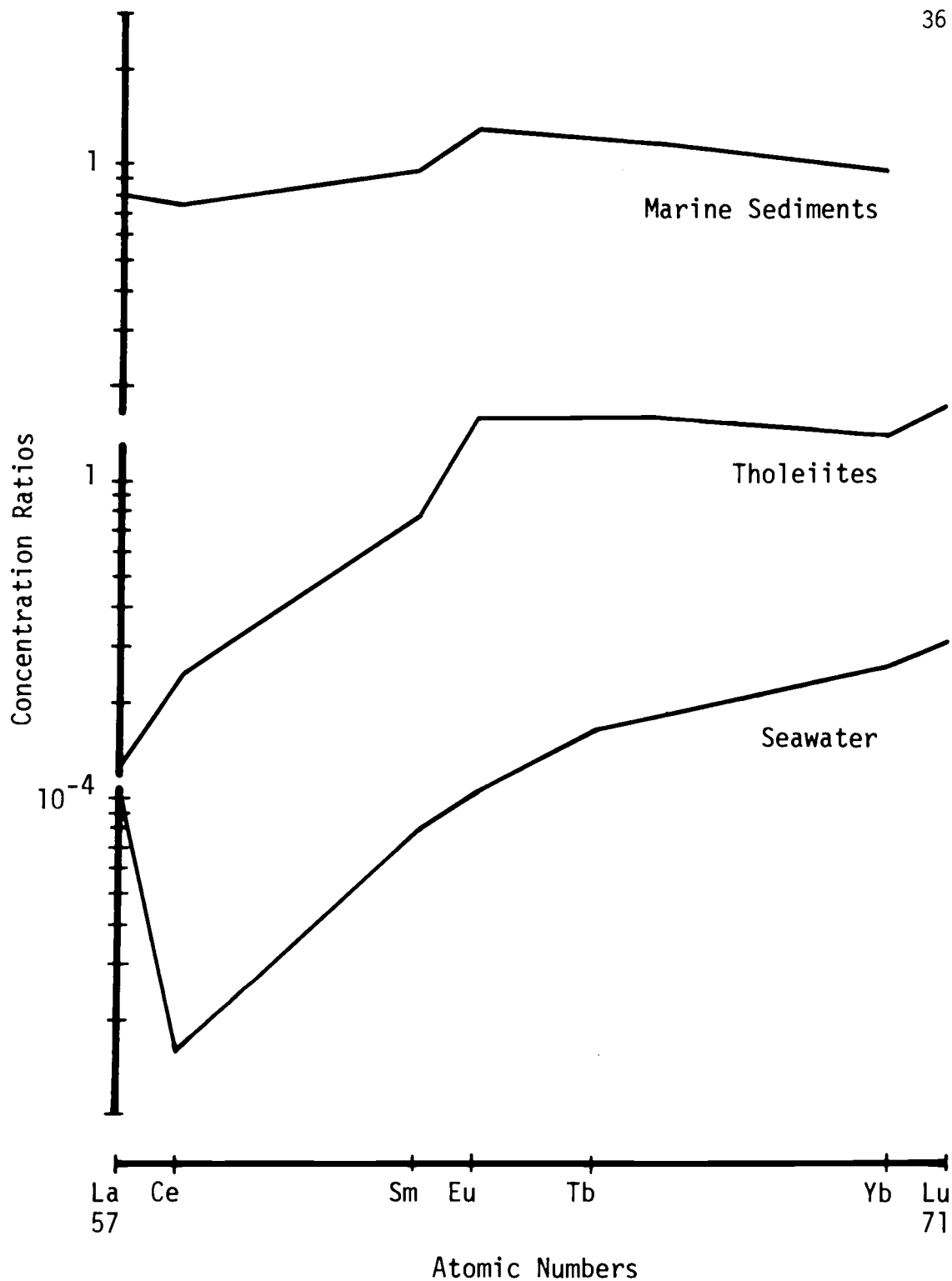


Figure 11. Shale normalized REE patterns of average seawater (Hogdahl et al., 1968), tholeiites (Frey and Haskin, 1964), and marine sediments (Wildeman and Haskin, 1965).

to that which is obtained by interpolating between La and Sm (Ce^*) (Ehrlich, 1967; Piper, 1974). This ratio (Ce/Ce^*) is then greater than 1.0 for cerium enrichment and less than 1.0 for cerium depletion. These ratios for the samples of this study vary from 0.03 to 2.28 (Table 3). They are extremely low in both iron (0.03-0.06) and manganese (0.04-0.48) hydrothermal crusts, being comparable to the average seawater value of Hogdahl et al. (1968) (0.16). They are also significantly less than 1.0 for most of the ferromanganese coatings and the manganese nodules from the EPR and Bauer Deep. The Equatorial Pacific nodules and a few of the ferromanganese coatings have Ce enrichments which are believed to be a common feature of manganese nodules.

The La/Ce ratios of these samples further illustrate the behavior of Ce. The La/Ce ratios of most hydrothermal samples are close to that of seawater ($La/Ce = 2.8$; Hogdahl et al., 1968), suggesting that they have incorporated small amounts of La and Ce from seawater with no subsequent enrichment of Ce. Ce enrichments, by preferential adsorption or other mechanism, are evident for ferromanganese crusts by their lower La/Ce ratios (generally < 1). The largest enrichments are found in the Equatorial and North Pacific nodules, which have La/Ce ratios near 0.25 (Figure 12).

Volatile Elements

No statistically significant correlations exist between the volatile elements Hg, As, Sb and Pb, in these samples. Even As and Sb, which often show strong geochemical coherence (Onishi and Sandell, 1955a and 1955b) show no correlation in these samples (Figure 13).

TABLE 3. Cerium Anomalies.

	Ce/Ce*	
Mn-rich Hydrothermal Crusts		
MN1749	0.19	
MN1846	0.19	
MN1848	0.04	
MN1850	0.06	
MN1896	--	
MN1750	0.10	
MN1751	0.47	
MN1752	0.10	
MN1776	0.48	
MN1809	1.91	
Fe-rich Hydrothermal Crusts		
MN1775	0.03	
MN1777	0.06	Ave. Seawater = 0.16 (Hogdahl et al., 1968)
Ferromanganese Coatings		
MN1194	0.32	
MN1626	0.57	
MN1627	0.67	
MN1628	1.56	
MN1629	1.63	
MN1630	0.30	
MN1657	0.16	
MN1659	0.40	
MN1660	0.56	
MN1768	1.65	
MN1845	--	Ce = measured Ce
MN1847	1.59	
MN1849	1.74	Ce* = Ce interpolated between La and Sm
Nodules		
MN1188	0.32	
MN1468	0.21	
MN1641	1.45	
MN1642	1.90	
MN1763	2.28	

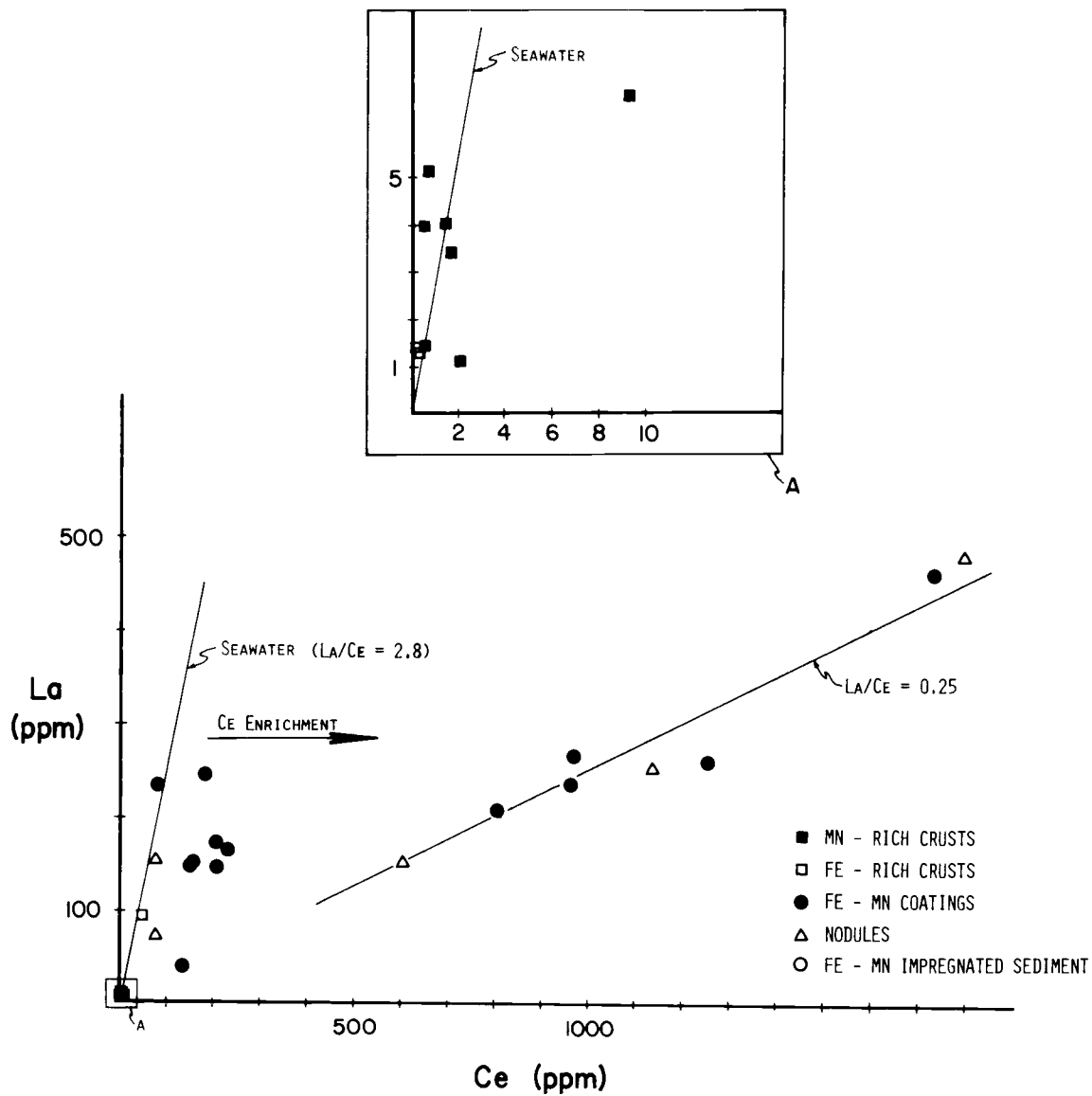


Figure 12. La vs. Ce concentrations. Hydrothermal crust La/Ce ratios are similar to seawater. All other deposits are enriched in Ce relative to seawater.

The following patterns, however, are evident for these elements.

Arsenic concentrations are high in nodules and ferromanganese coatings. The hydrothermal iron-rich crusts also have remarkably high concentrations of As, much greater than other minor elements. The Mn hydrothermal crusts, on the other hand, have very low As concentrations, in line with their low abundances of other minor elements. An apparent correlation between Fe and As was noticed by Cronan (1972) in sediments from the median valley of the MAR, and this correlation appears to exist for all ferromanganese deposits of this study (see Figure 14).

Antimony concentrations range in a rather unsystematic manner from a low of 3 ppm in an iron-rich crust (MN1777) to a high of greater than 150 ppm in two manganese-rich crusts (MN1848 and MN1850) and one ferromanganese coating (MN1768). Even though Sb is low in the iron-rich crusts, its behavior is quite unlike that of the minor elements, having values in some of the very "pure" manganese-rich crusts greater than or equal to those ferromanganese nodules and coatings.

Mercury concentrations in ferromanganese deposits are very low, but highly variable, as originally found by Harriss (1968). In his study, Harriss found nodule concentrations to range from 1 to 800 ppb. The Hg concentrations in the samples of this study range even further, from 3 to 2520 ppb. This wide range, however, results from the wide range of concentrations in ferromanganese coatings and manganese-rich crusts, as illustrated in Figure 15. The nodules analyzed have uniformly low mercury content.

Very high Hg concentrations were found in samples from two

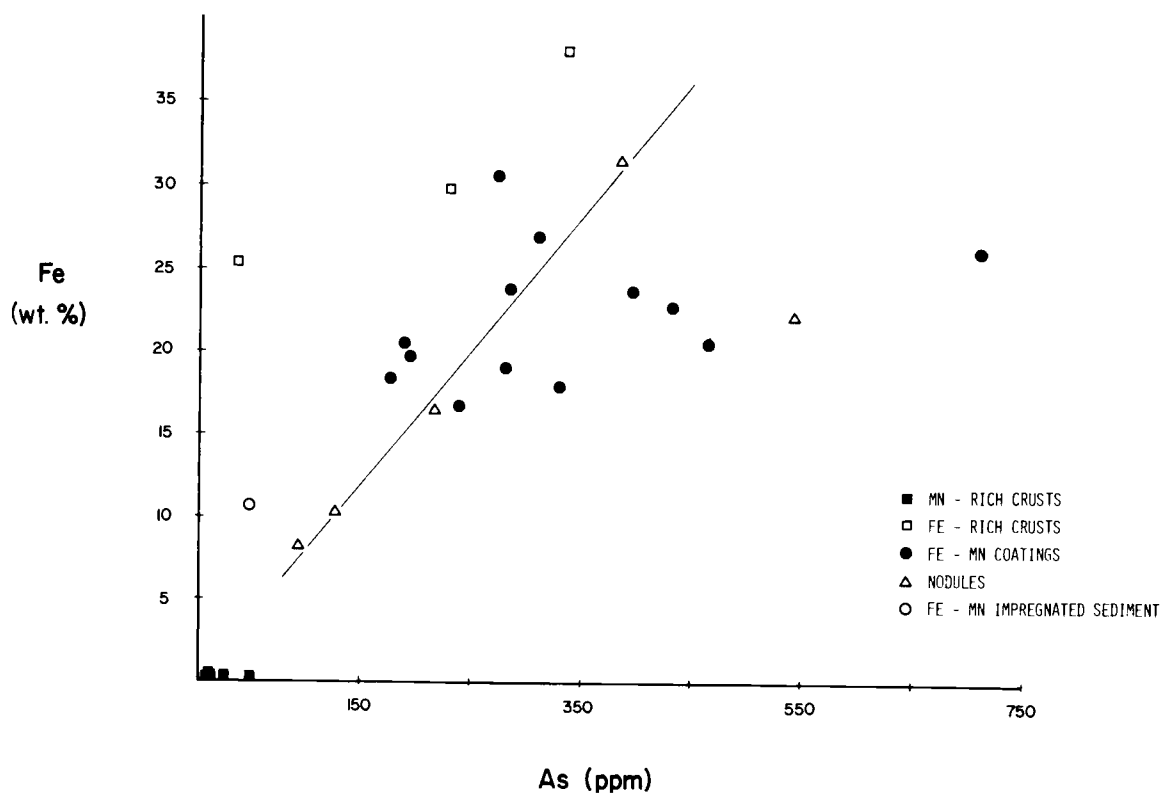


Figure 14. Fe vs. As concentrations showing the high As concentrations in Fe-rich crusts and correlation of Fe and As in most ferromanganese deposits.

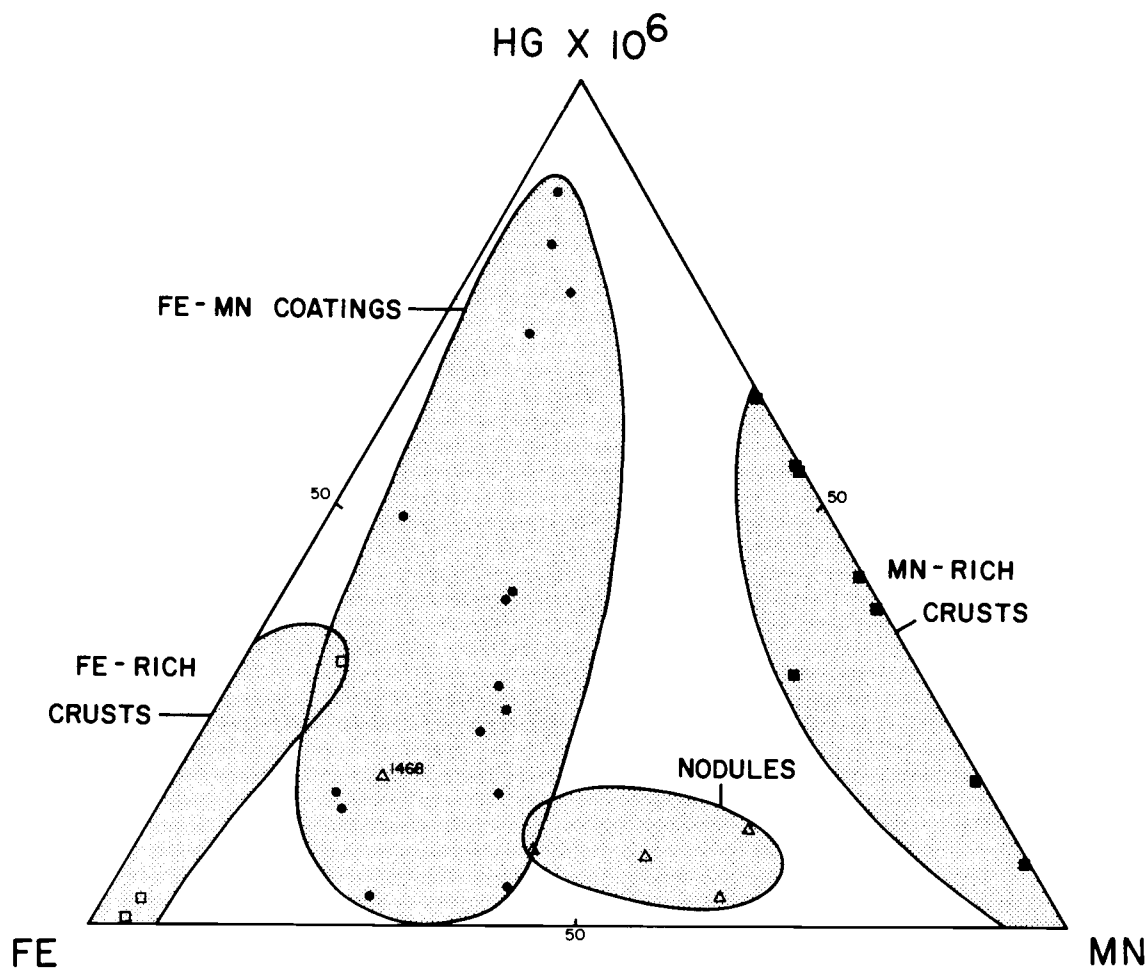


Figure 15. Ternary diagram of Fe vs. Mn vs. Hg showing the wide range of Hg concentrations in ferromanganese coatings and Mn-rich crusts.

locations, the AMPH D6 iron and manganese samples and the TAG hydrothermal and ferromanganese samples. Of the TAG samples, the ferromanganese coatings have far higher Hg contents. Mercury is high in both phases of the AMPH D6 sample, but much greater in the manganese phase.

Lead concentrations in these samples are also highly variable. The highest values are found in two Pacific nodules (MN1641 and MN1642), a ferromanganese coating (MN1628) and the manganese-rich phase of the AMPH D6 sample (all > 2000 ppm). Most ferromanganese coatings have lead concentrations nearly an order of magnitude less than these. Very low lead values are found for the manganese and iron hydrothermal crusts (generally < 10 ppm). In general, lead concentrations are similar to those of the trace metals -- greater in nodules than in ferromanganese coatings, and very low in hydrothermal crusts.

With the exception of lead, the volatile element concentrations bear no resemblance to the general trend shown by most minor elements. Instead, the concentrations of Hg, As and Sb are highly variable, with occasional anomalously high values in hydrothermal crusts and ferromanganese coatings. The fact that these anomalous values are found only in deposits from volcanically active areas suggests that the source for these elements may be ridge volcanism. Direct evidence of such a source for mercury has been found near the FAMOUS dive site on the MAR, where anomalously high mercury concentrations have been measured in the bottom water (Carr et al., 1975).

DISCUSSION

Hydrothermal Crusts: Major Element Composition

Marine hydrothermal deposits are characterized by extreme Fe/Mn values Fe and Si contents which co-vary, and generally very low concentrations of trace metals and REE. The chemical stability limits of dissolved silica and the oxides of iron and manganese indicate that silica and iron will precipitate before manganese in an environment of increasing pH and oxidation potential, and decreasing temperature, as would be encountered upon mixing of a hydrothermal fluid with oxygenated bottom water. These crusts therefore appear to represent two end members of the fractional precipitation of hydrothermal fluids containing large amounts of dissolved iron, silica and manganese.

The fractionation of iron and manganese can be easily explained by the lower solubility of iron species as both iron and manganese undergo oxidation (Krauskopf, 1957). The nearly 1:1 correlation of Si with Fe (Figure 2), however, is less well understood. Submarine hydrothermal solutions are believed to have very high Si/Fe ratios. Si/Fe ratios in solutions resulting from the interaction of seawater and basalt at elevated temperatures (200-500°C) (Hajash, 1975; Bischoff and Dickson, 1975; Seyfried and Bischoff, 1977), and in a thermal brine from the Reykjanes Peninsula (temp. = 277°C) (Mottl et al., 1975) range from 10 to >500. Mixture of such a solution with normal seawater in a 1:1 ratio results in the precipitation of an amorphous silica-hydrated iron oxide deposit, highly dominated by silica (Seyfried and Bischoff, 1977). However, mixture with large amounts of seawater can cause the dilution of dissolved silica below the amorphous silica saturation concentration, resulting in the lone precipitation of iron (Seyfried and

Bischoff, 1977). Hydrothermal deposits with highly variable Si/Fe ratios would therefore be expected.

Other experimental evidence, however, indicates that the deposition of amorphous silica and hydrated iron oxide are not independent, as suggested by the results of Seyfried and Bischoff. Harder and Flehmig (1970) have found that SiO_2 is adsorbed onto colloidal iron hydroxide from solutions highly undersaturated with respect to amorphous silica. The resulting X-ray amorphous precipitates are rich in both Fe and SiO_2 . This may be an important mechanism for the formation of the Fe-Si crusts of this study.

The deposition of hydrothermal iron and silica can apparently take two forms: 1) amorphous silica and hydrated iron oxides and 2) iron-rich smectite or nontronite. It is not surprising to find either of these phases associated with hydrothermal deposits. Amorphous hydrated iron oxide is the most common form of iron in ferromanganese deposits. Nontronite and other smectites are thought to form both as low-temperature alteration products in oceanic basalts, as well as from higher temperature interaction of seawater with cooling basalt (Bischoff and Dickson, 1975; Hajash, 1975). Two factors exist which may determine which of these two forms is present, 1) the chemical environment of deposition, and 2) diagenetic processes. Although smectite may form diagenetically in many locations, such as the Bauer Basin (Heath and Dymond, 1977), there is evidence that smectite precipitates directly in deposits from other locations. Direct precipitation of iron-rich nontronite is apparently presently occurring in the Atlantis II deep of the Red Sea geothermal system (Bischoff, 1969; Bischoff, 1972). Though the Red

Sea system is not identical to mid-ocean ridge hydrothermal systems, the physiochemical environment of the Atlantis II brine may be similar to that near the mouth of a mid-ocean hydrothermal vent (i.e. elevated temperatures, low pH, high Fe^{+2} , SiO_2 and Mn^{+2} concentrations). Direct precipitation of hydrothermal smectite does therefore appear possible.

The chemical environments which favor the precipitation of either smectite or amorphous iron and silica are difficult to ascertain. The wide occurrence of smectite, of presumable authigenic origin, in marine sediments suggests that it is a thermodynamically stable phase in the normal marine environment. Its formation, therefore, may be favored by relatively slow precipitation under near-normal seawater conditions. Amorphous silica and hydrated iron oxide are common, rapidly forming, low temperature precipitates from Fe and Si-rich solutions. Their precipitation may be favored in an environment of rapid deposition in an early stage of deposition, during the initial reaction of seawater and hydrothermal fluid.

The chemical compositions and mode of occurrence of the iron-rich crusts support these ideas. The smectite sample (MN1777) was deposited on the open sea floor (Michel Hoffert, pers. comm.) and contains a small amount of late-forming MnO_2 . Of the two amorphous deposits, one (MN1727) occurs as a vein filling, and the other (MN1775) is nearly pure iron and silica, both features which suggest early stage deposition.

The manganese-rich crusts are composed of birnessite and todorokite of unusually high purity and crystallinity. These features are undoubtedly related to the physio-chemical environment of deposition of the crusts, but just how is not clear. The fractional precipitation of

Fe and Mn is probably a small scale process. It may occur only in response to special circumstances, where the mixture of a hydrothermal solution with seawater is hindered by flowing through an obstacle such as sediment or a submarine talus deposit. Under such conditions, Mn is able to precipitate under fairly stable conditions, from a solution of rather high concentration (probably several ppm, based on the data of Seyfried and Bischoff, 1977) onto an available solid surface. Such a situation may favor the formation of more ordered crystalline phases.

Hydrothermal Crusts: Minor Element Composition

Minor element concentrations in ferromanganese deposits are controlled, to a first approximation, by adsorption onto MnO_2 and $FeOOH$ surfaces. The adsorption process can be considered a combination of electrostatic attraction and specific chemical adsorption (Murray, 1973), and is therefore dependent on 1) the degree of specific chemical adsorption, 2) the concentration and charge density of ions in solution, 3) the pH of the solution, and 4) the time available for diffusion of ions to the adsorbing surface. The accumulation of minor elements, in general, in hydrothermal crusts is inhibited by the latter two of these factors. The surface charges of MnO_2 and $FeOOH$ species are pH dependent, and their pH of zero point charge, $pH(ZPC)$, are at $pH = 2-3$ (Stumm and Morgan, 1970) and $7-9$ (Murray, 1973), respectively. Anomalously low pH is one of the most outstanding characteristics of seawater that has been altered by hydrothermal activity. Low pH values, of from $3-5$, are found to extend over wide areas surrounding shallow water hydrothermal systems (Honnorez et al., 1973; J. Dymond and E. J. Dasch, pers.

comm.). Under such pH conditions, the negative surface charge of MnO_2 is reduced and that of $FeOOH$ may be positive. Their ability to adsorb cations from both seawater and hydrothermal solution is therefore diminished.

The relatively rapid accumulation rates of the hydrothermal deposits also inhibit accumulation of minor elements from very dilute solution. There is simply not sufficient time available for large numbers of ions to be adsorbed. It is therefore possible that enrichments of minor elements, relative to normal seawater, exist in hydrothermal solutions, and yet these elements are not readily incorporated into the deposits that form from these solutions.

The affect of these two factors will be overcome if trace metal concentrations in hydrothermal solutions are significantly greater than seawater. At high concentrations (10^{-3} - 10^{-4} M) all transition metal ions rapidly adsorb on δMnO_2 , even at pH below $pH(ZPC)$ (Murray, 1973).

Are significant concentrations of trace metals likely in hydrothermal solutions? Experimental and field studies suggest that it is possible, but they are not conclusive. Mottl et al. (1975) were unable to detect Cu, Ni or Zn (detection limit = 0.1 ppm) in thermal brine from the Reykjanes Peninsula. Cu, but not Ni was detected in some of Hajash's high temperature (400-500°C) seawater-basalt leaching experiments. Bischoff and Dickson (1975) found Cu and Ni, but not Zn or Pb to be slightly solubilized by leaching at 200°C. Most recently Seyfried and Bischoff (1977) found Zn, Cu and Ba to be enriched in experiments at 200°C using large seawater/basalt ratios.

In the above experimental and field results, when trace metals were detected, their concentrations were low (in almost all cases, significantly less than 1 ppm). This is undoubtedly related to the low concentrations of trace metals in tholeiitic basalts, which are approximately 10^{-2} that of manganese and 10^{-4} that of iron.

An additional factor, which may lower the trace metal content of hydrothermal solutions, is the partitioning of trace metals into hydrothermal sulfide phases within the oceanic crust. Precipitation of hydrothermal sulfide minerals is known to occur at locations of shallow water submarine volcanism (Honnorez et al., 1973) and is believed to be occurring in hydrothermal systems within the ocean crust (Bonatti, 1975). Because trace metals such as Cu, Ni and Zn are known to be strongly partitioned into sulfide phases in siliceous melts (MacLean and Shimazaki, 1976), the precipitation of these phases may be an effective mechanism for their removal from hydrothermal solutions. Trace metals therefore may be brought into solution in the initial stages of the hydrothermal system, but precipitate as sulfides under reducing conditions within the oceanic crust before emanation of the fluid onto the sea floor.

From the above discussion, it is evident that the existence of significant amounts of trace metals in hydrothermal solutions emanated onto the sea floor is still in doubt. Variations in the physical and chemical parameters of individual systems (i.e. temperature, pressure, water/rock ratio), as well as rock composition, appear to result in solutions with highly variable trace metal content. The small amounts of trace metals that are found in hydrothermal deposits therefore may originate from hydrothermal solutions, the surrounding seawater, or both.

A strong inverse correlation exists between growth rates of ferromanganese deposits (including hydrothermal deposits) and concentrations of the trace metals Co, Ni, and Cu (M. R. Scott, pers. comm.). This correlation suggests the accumulation of these elements from a single, constant source -- normal seawater. The uniformly low concentrations of these elements in the hydrothermal crusts of this study are therefore believed to originate by adsorption from seawater.

The relative accumulation rates of these three elements in most ferromanganese deposits appear to result from a combination of 1) their degree of selective adsorption, and 2) their seawater concentrations. Adsorption of trace metals in ferromanganese deposits occurs predominantly onto MnO_2 , as found by experimental work of Krauskopf (1956) and as indicated by the positive correlation of Co, Ni, and Cu with Mn in massive ferromanganese deposits (Burns and Brown, 1972). Their selectivity of adsorption onto δMnO_2 has been determined by Murray et al. (1968) to be, $Co > Ni \approx Cu$. Seawater concentrations (Brewer, 1975) are of the order $Ni > Cu > Co$. These result in the relative accumulation in ferromanganese deposits of $Co \approx Ni > Cu$ (M. R. Scott, Pers. Comm.).

The hydrothermal crusts of this study are unusual in that they are depleted in Co relative to Ni and Cu (the relative concentrations therefore are $Ni > Cu > Co$). High Co concentrations in slowly forming ferromanganese deposits are undoubtedly related to the remarkably high specific adsorption of Co^{+2} onto MnO_2 , as measured by Murray et al. (1968), Loganathan and Bureau (1973) and Murray (1973). This specific adsorption has been attributed by various authors to Co^{+2} replacement of

structurally bound Mn^{+2} and Mn^{+3} (Loganathan and Burau, 1973) or oxidation of adsorbed Co^{+2} to Co^{+3} and replacement of Mn^{+4} (Burns, 1974). At seawater Co concentrations ($\sim 10^{-9}M$ (Brewer, 1975)), these replacement processes may be slow relative to the accumulation rates of the hydrothermal crusts, resulting in low Co concentrations in these deposits.

The REE, with a few exceptions, also appear to have a seawater source in these deposits. Both the very low absolute concentrations and characteristic La/Ce ratios (Figure 12) are consistent with this interpretation. In the TAG samples, the correlation of REE with seawater values exists for the entire rare-earth series (Figure 9). Conspicuous Sm and Lu anomalies have been found in some of these samples. These may be the result of analytical uncertainties at the low concentrations being measured. If these anomalies are real, however, they must result from preferential incorporation of Sm and Lu from seawater, or incorporation from an additional source. Since no mechanism is known by which Sm and Lu are preferentially incorporated into iron and manganese oxides, another source, possibly hydrothermal solutions, is likely.

The similarity of the La/Ce ratios in these deposits to that of seawater is actually quite surprising. Ce is preferentially incorporated from seawater into all other ferromanganese deposits. Enrichment of Ce occurs by preferential adsorption onto iron and manganese oxide surfaces due to the greater charge density of the Ce^{+4} ion than those of the trivalent REE, and possibly other properties specific to Ce. Additional fractionation of Ce into manganese phases may also occur as a result of diagenetic reactions in the sediment. Evidence for the

uptake of REE in fish bone apatite, after deposition in sediments, has been found by Arrhenius and Bonatti (1965) and Arrhenius et al. (1957). Ce is excluded in this uptake (La/Ce values in fish bone apatite in marine sediments range from 1.0 (Arrhenius and Bonatti, 1965) to 100 (Eklund, 1974)) and may incorporate into the manganese phases which form nodules (Arrhenius and Bonatti, 1965). This diagenetic fractionation of Ce would account for the greater Ce enrichment in nodules versus ferromanganese coatings.

Zn, As, Sb and Hg are elements which have anomalously high concentrations in many of the hydrothermal crusts. With the possible exception of As, there are no known mechanism by which these elements can be preferentially incorporated into these deposits from normal seawater. It is therefore believed that an additional source of these elements -- hydrothermal solutions -- are responsible for their high concentrations.

The recent experimental study of Seyfried and Bischoff (1977), of the high temperature and pressure (200°C, 500 bars) interaction of seawater and basaltic glass, found Zn (besides Fe and Mn) to be the trace metal taken into solution in highest concentration. The predominance of Zn over other trace metals in their study, and in hydrothermal solutions emanating onto the sea floor, may result from two factors: 1) Zn concentrations in many tholeiitic basalts are greater than those of other trace metals, and 2) as compared to Co, Cu and Ni, Zn has the lowest affinity for sulfide phases (MacLean and Shimazaki, 1976), which may remove these elements from solution.

The existence of anomalously high concentrations of Hg, As and Sb in some hydrothermal crusts and ridge-crest ferromanganese coatings

suggests that these elements are associated with submarine volcanism. High concentrations of these elements in terrestrial thermal springs, and their general enrichment in sediments and sedimentary rocks have led to the widely excepted view that these elements are escaping from the earth in thermal springs associated with volcanic exhalations. The large scale input of iron and manganese to the oceans via submarine hydrothermal processes, however, suggests that hydrothermal leaching may be a more likely source for these elements.

The concentrations of these elements in basalts are very low ($\text{Hg} \approx 100$ ppb, As and $\text{Sb} \leq 2$ ppm) (Turekian and Wedepohl, 1961), but two processes may enhance their ability to be leached by hydrothermal solutions: 1) their volatility determines that they are among the last of the elements to enter into crystalline phases in a cooling magma. They thus occupy sites, such as intergranular boundaries, easily accessible to leaching. 2) Their ability to form strong chloride complexes may enhance their ability to be leached by submarine hydrothermal chloride brines.

These ideas are supported by recent experimental evidence in which significant quantities of As and Sb have been leached from volcanic and sedimentary rock by hot water at 200° - 400°C (Ewers, 1977).

With the exception of Si and Fe , As and Fe are the only two elements which correlate to any degree in all of the samples of this study (Figure 14). The chemical affinity of As for Fe , and specifically of As in solution for hydrated iron oxide is evidenced by both experimental studies (Hem and Skougstad, 1960) and the correlation of As and Fe in marine metalliferous sediments (Cronan, 1972) and terrestrial

ore deposits (Hem and Skougstad, 1960). This affinity may result in part from the electrostatic attraction of As, which exists as the HAsO_4^{-2} and $\text{H}_2\text{AsO}_4^{-}$ anions in seawater (Brewer, 1975), to positively charged hydrated iron oxide colloids. This type of attraction has been hypothesized to account for the adsorption of many anionic species from seawater by hydrated iron oxide (Goldberg, 1954). The adsorption of As is undoubtedly more specific than simple electrostatic attraction, but the specific chemical mechanism is, as yet, not known.

Ferromanganese Coatings and Nodules

Ferromanganese coatings formed on basalt outcroppings on the EPR, MAR and Juan de Fuca Ridge have been found to be similar in composition to metalliferous sediments occurring on the EPR. Their similar locations (on mid-ocean ridges) and compositions, characterized by enrichments of Fe and Si, and depletion of trace metals relative to manganese nodules, suggest that they have a common origin. Figures 1, 2, and 6 suggest that their compositions may be accounted for by a "dilution" of normal seawater or "hydrogenous" (Bonatti et al., 1972c) deposition (represented by nodules) by hydrothermal Fe and Si. Accumulation rates, however indicate that hydrogenous or "normal authigenic" precipitation can play only a minor role in the accumulation of either Fe or Mn in EPR metalliferous sediments (Dymond and Veeh, 1975). The majority of the Fe and Mn in these sediments, and presumably ferromanganese coatings, comes from precipitation from hydrothermal solutions.

It is probable that only a small amount of the Fe, SiO₂ and Mn contained in hydrothermal solutions is locally precipitated as iron and manganese-rich crusts. The majority of these constituents undoubtedly form amorphous, or nearly amorphous, colloids or remain in solution (Seyfried and Bischoff, 1977), to be advected by bottom currents. These colloids can be transported large distances, and are consequently mixed and homogenized, thus destroying local fractionation effects and variability in the compositions of individual hydrothermal systems. They eventually precipitate as ferromanganese coatings and metalliferous sediments. Large amounts of minor and trace elements are adsorbed by the colloidal iron and manganese before their final deposition. These deposits may also be modified by hydrogenous, biogenous and detrital contributions (Heath and Dymond, 1977).

The mineralogy of the ferromanganese coatings (poorly crystalline δMnO₂) is consistent with an origin of precipitation of colloidal Fe, SiO₂ and Mn. It has also been recently suggested (Heath and Dymond, 1977) that the authigenic phases which make up EPR metalliferous sediments, iron-rich smectite, todorokite, and a ferromanganese micro-laminated phase (Eklund, 1974), have formed diagenetically from amorphous iron and manganese oxides and silica.

Manganese nodule composition is characterized by enrichment of minor elements and manganese beyond that of ferromanganese coatings and metalliferous sediments. Recently, it has become increasingly evident that variations in nodule compositions are not determined simply by variations in authigenic precipitation of metals from seawater. The compositional variations in nodule tops and bottoms (Raab, 1974),

the mobility of elements in the sedimentary column (Bender, 1971), and recent theories of diagenetic partitioning of iron and manganese in sediments (Heath and Dymond, 1977 ; Lyle et al., 1977) suggest that processes at the sediment-seawater interface are involved. If the compositions of ferromanganese coatings and metalliferous sediments are considered to represent hydrothermal iron and manganese which has adsorbed trace elements from seawater, nodule compositions may result from enrichment of this material in manganese and trace metals by one of two diagenetic processes: 1) partitioning of the iron, manganese and trace metals into iron-rich smectite and manganese and trace metal-rich todorokite (Lyle et al., 1977), or 2) mobilization of manganese and trace metals out of the sedimentary column and incorporation into nodules.

CONCLUSIONS

The fractional precipitation of submarine hydrothermal solutions has been found to result in the formation of two, distinct end member deposits:

- 1) highly crystalline birnessite or todorokite crusts, with generally very low trace metal content, variable content of mercury, arsenic and antimony, and cerium-depleted rare earth patterns which are similar to seawater or erratic.
- 2) iron and silica-rich crusts composed of iron-rich nontronite or amorphous hydrated iron oxides and silica, also with very low trace metal contents (but high arsenic concentrations) and erratic rare earth patterns with strong cerium depletions.

The fractionation of iron and manganese occurs as a result of the lower solubility of iron species as both iron and manganese undergo oxidation (Krauskopf, 1957) by mixing of the reduced hydrothermal fluid with oxygenated bottom water. The coherence of Si and Fe may result from co-precipitation or adsorption of dissolved SiO_2 onto hydrated iron oxide colloids.

The low content of minor elements such as Co, Ni, Cu, Pb and Ba in these deposits results from three factors: 1) the low concentrations of these elements in hydrothermal solutions, 2) the rapid deposition of these deposits (which minimizes adsorption of elements from seawater), and 3) the possible reduced adsorption of minor elements under low pH conditions of deposition.

The cerium depletions in the REE patterns of the hydrothermal crusts, which are similar to those of seawater, are believed to result

from the incorporation of small amounts of REE from seawater. Other anomalies in the REE patterns may be due to incorporation of REE mobilized by hydrothermal leaching, although analytical uncertainties makes these anomalies questionable.

Anomalously high Zn, As, Sb and Hg contents of some hydrothermal crusts suggest that these elements are input to the ocean by some hydrothermal systems.

Zinc may be enriched in hydrothermal solutions relative to other trace metals because of its higher concentrations in tholeiitic basalts and its low affinity for sulfide phases. Precipitation of sulfide minerals within the oceanic crust may remove other trace metals from solution before emanation onto the sea floor. Two processes which may enable significant amounts of Hg, As and Sb to be solubilized by hydrothermal leaching are: 1) their volatility determines that they are among the last of the elements to incorporate into crystalline phases in a cooling magma. They thus occupy sites, such as intergranular boundaries, easily accessible to leaching. 2) Their ability to form strong chloride complexes may enhance their ability to be leached by submarine hydrothermal chloride brines.

From the data of this study, a model for the deposition of hydrothermal iron and manganese is proposed which involves,

- 1) the fractionation of a small percentage of iron, manganese and silica in hydrothermal solution, into amorphous iron hydroxide and silica, or iron-rich nontronite, and highly crystalline birnessite or todorokite.

- 2) precipitation of the majority of these elements as hydrated colloids which remain in suspension to be advected by bottom currents. While in suspension the iron and manganese colloids adsorb minor elements from seawater, and eventually precipitate as metalliferous sediments and ferromanganese coatings.

Figure 16 summarizes the processes that are involved in the deposition of these phases.

Manganese nodule compositions may be determined by enrichment of the Fe-Mn colloidal material in manganese and trace elements by diagenetic processes.

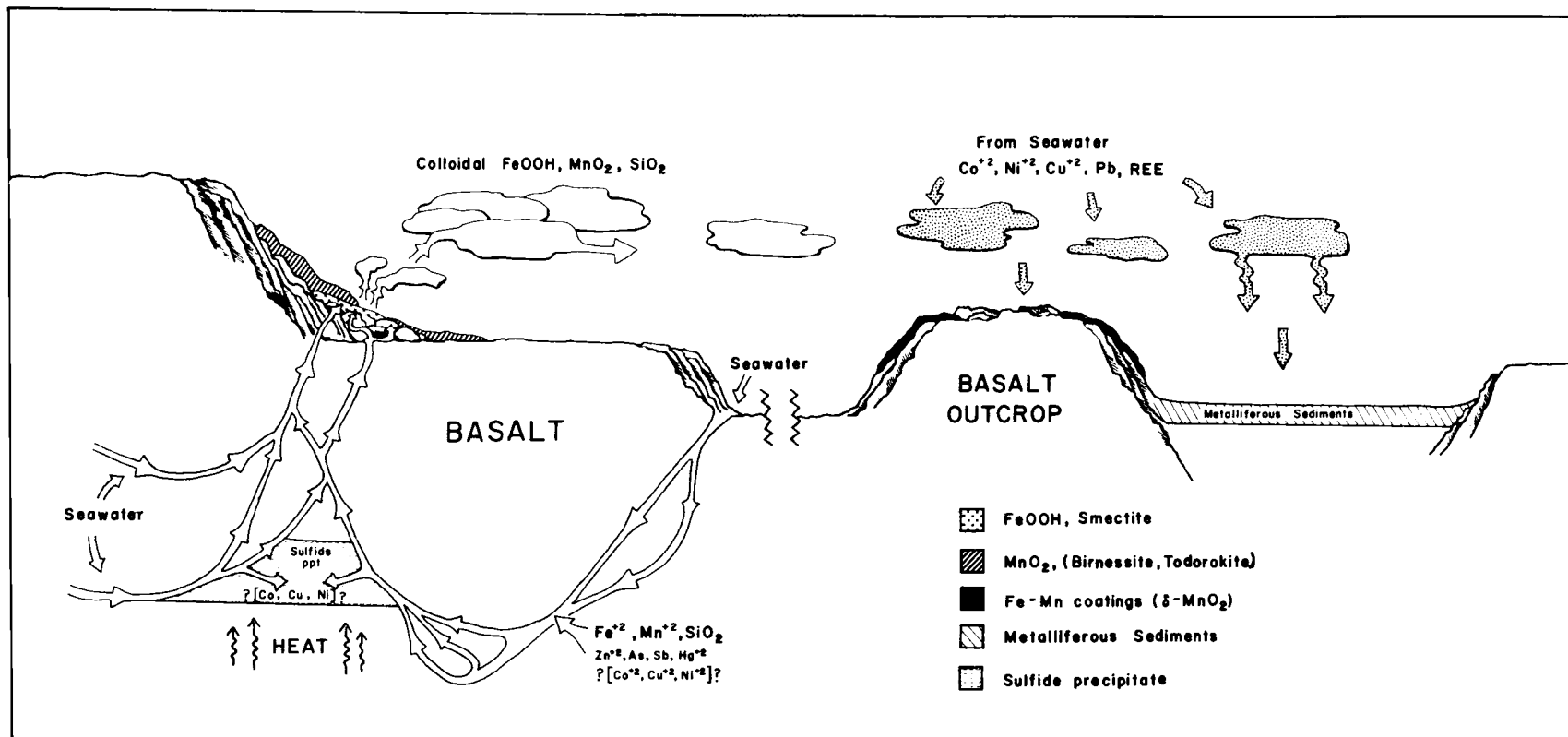


Figure 16. Illustration summarizing the processes involved in the deposition of Fe and Mn-rich hydrothermal crusts, ferromanganese coatings and metalliferous sediments.

BIBLIOGRAPHY

- Arrhenius, G. and Bonatti, E., 1965. Neptunism and volcanism in the ocean. In: Progress in Oceanography, v. 3, ed. M. Sears. Pergamon Press Ltd., p. 7-23.
- Arrhenius, G., Bramlette, M. N., and Picciotto, E., 1957. Localization of radioactive and stable heavy nuclides in ocean sediments. Nature, v. 180, p. 85-86.
- Bender, M. L., 1971. Does upward diffusion supply the excess manganese in pelagic sediments? J. Geophys. Res., v. 76, p. 4212-4215.
- Bender, M. L., Broecker, W., Gornitz, V., Middel, U., Kay, R., Sun, S. S., and Biscaye, P., 1971. Geochemistry of three cores from the East Pacific Rise. Earth Planet. Sci. Lett., v. 12, p. 425-433.
- Bischoff, J. L., 1969. The Red Sea geothermal deposits: Their mineralogy, chemistry, and genesis. In: Hot Brines and Recent Heavy Metal Deposits in the Red Sea, ed. E. T. Degens and D. Ross. Springer, New York, p. 368-401.
- Bischoff, J. L., 1972. A ferroan nontronite from the Red Sea geothermal system. Clays and Clay Mins., v. 20, p. 217-223.
- Bischoff, J. L. and Dickson, F. W., 1975. Seawater-basalt interactions at 200°C and 500 bars: implications for origin of heavy metal deposits and regulation of seawater chemistry. Earth Planet. Sci. Lett., v. 25, p. 385-397.
- Bonatti, E., 1975. Metallogensis at oceanic spreading centers. In: Annual review of Earth and Planetary Sciences. Annual Reviews, Inc., p. 146-166.
- Bonatti, E., Fisher, D. E., Joensuu, O., Rydell, H. S., Beyth, M., 1972a. Iron-manganese-barium deposit from the northern Afar Rift (Ethiopia). Econ. Geol., v. 67, p. 717-730.
- Bonatti, E., Honnorez, J., Joensuu, O., Rydell, H., 1972b. Submarine iron deposits in the Mediterranean Sea. In: The Mediterranean Sea, ed. D.J. Stanley. Dowden, Hutchinson & Ross, p. 701-710.
- Bonatti, E., Kraemer, T., Rydell, H., 1972c. Classification and genesis of submarine iron-manganese deposits. In: Ferromanganese Deposits on the Ocean Floor, ed. D. Horn. Nat. Sci. Found., p. 149-165.

- Bostrom, K. and Fischer, D. E., 1969. Distribution of mercury in East Pacific sediments. *Geochim. Cosmochim. Acta.*, v. 33, p. 743-745.
- Bostrom, K. and Peterson, M.N.A., 1966. Precipitates from hydrothermal exhalations on the East Pacific Rise. *Econ. Geol.*, v. 61, p. 1258-1265.
- Bostrom, K. and Peterson, M.N.A., 1969. The origin of aluminum-poor ferromanganean sediments in areas of high heat flow on the East Pacific Rise. *Mar. Geol.*, v. 7, p. 427-447.
- Bostrom, K. and Valdes, S., 1969. Distribution of arsenic in deep-sea sediments and rocks. *Lithos*, v. 2, p. 351.
- Brewer, P. G., 1975. Minor elements in sea water. In: *Chemical Oceanography*, v. 1, 2nd ed., ed. J. P. Riley and G. Skirrow, Academic Press, p. 415-496.
- Brown, B. A., 1972. A low-temperature crushing technique applied to manganese nodules. *Am. Mineral.*, v. 57, p. 284-287.
- Burns, R. G., 1976. The uptake of cobalt into ferromanganese nodules, soils and synthetic manganese (IV) oxides. *Geochim. Cosmochim. Acta*, v. 40, p. 95-102.
- Burns, R. G. and Brown, B. A., 1972. Nucleation and mineralogical controls on the composition of manganese nodules. In: *Ferromanganese deposits on the ocean floor*, ed. D. Horn. IDOE Publication, p. 51-61.
- Burns, R. G. and Burns, V. M., 1975. Mechanism for nucleation and growth of manganese nodules. *Nature*, v. 255, p. 130-131.
- Burns, R. G. and Burns, V. M., 1977. Mineralogy of ferromanganese nodules. In: *Marine Manganese Deposits*, ed. G. P. Glasby, in press.
- Carr, R. A., Jones, M. M., Warner, T. B., Cheek, C. H., and Russ, E. R., 1975. Variations in time of mercury anomalies at the Mid-Atlantic Ridge. *Nature*, v. 258, p. 588-589.
- Christmann, D. and Ingle, J. R., 1976. Problems with sub-ppb mercury determinations: preservation of standards and prevention of water mist interferences. *Anal. Chimica Acta*, v. 86, p. 53-62.
- Corliss, J. B., 1971. The origin of metal-bearing hydrothermal solutions. *J. Geophys. Res.*, v. 76, pp. 8128-8138.
- Corliss, J. B. and Dymond, J., 1975. Nazca Plate metalliferous sediments: I. Elemental distribution patterns in surface samples. *EOS (Amer. Geophys. Union Trans.)*, n. 56, p. 445.

- Cotton, F. A. and Wilkinson, G., 1972. *Advanced Inorganic Chemistry*. Interscience, New York, p. 1057.
- Crane, K. and Normark, W. R., 1975. Ridge crest structure vs. hydrothermal activity. (East Pacific Rise 21°N). *Trans. Amer. Geophys. Union, (EOS)*, v. 13, p. 175.
- Cronan, D. S., 1972. The Mid-Atlantic Ridge near 45°N, XVII: Al, As, Hg, and Mn in ferruginous sediments from the median valley. *Can. J. Earth. Sci.*, v. 9, p. 319-323.
- Dasch, E. J., Dymond, J. R., and Heath, G. R., 1971. Isotopic analysis of metalliferous sediment from the East Pacific Rise. *Earth Planet. Sci. Lett.*, v. 13, p. 175-180.
- Dymond, J. R., Corliss, J. B., Heath, G. R., Field, C. W., Dasch, E. J., and Veeh, H. H., 1973. Origin of metalliferous sediments from the Pacific Ocean. *Geol. Soc. Am. Bull.*, v. 84, pp. 3355-3372.
- Dymond, J. R. and Veeh, H. H., 1975. Metal accumulation rates in the Southeast Pacific and the origin of metalliferous sediments. *Earth Planet. Sci. Lett.*, n. 27, p. 241-248.
- Enrlich, A. M., 1968. Rare-earth abundances in manganese nodules. Ph.D. Dissertation, M. I. T., Dept. of Chem., 222 p.
- Eklund, W. A., 1974. A microprobe study of metalliferous sediment components. Unpublished M. S. Thesis, Oregon State University, 77 p.
- Elder, J. W., 1965. Physical processes in geothermal areas. In: *Terrestrial Heat Flow, Am. Geophys. Un. Mono.*, no. 8, p. 211.
- Ewers, G. R., 1977. Experimental hot water-rock interactions and their significance to natural hydrothermal systems in New Zealand. *Geochim. Cosmochim. Acta*, v. 41, p. 143-150.
- Ferguson, J. and Lamberg, I. B., 1972. Volcanic exhalations and metal enrichments at Matupi Harbor, New Britain, T. P. N. G., *Econ. Geol.*, v. 67, p. 25-37.
- Goldberg, E. D., 1961. Chemistry in the oceans. In: *Oceanography*, ed. M. Sears. AAAS publ. 67, p. 583-597.
- Goldberg, E. D., Koide, M., Schmitt, R., Smith, R., 1963. Rare earth distributions in the marine environment. *J. Geophys. Res.*, v. 68, p. 4209-4217.
- Goldschmidt, V. M., 1954. *Geochemistry*. Clarendon Press, Oxford, 730 p.

- Gundlach, H., Beiersdorf, H., Marchig, V., and Schnier, C., 1976. "Heated" bottom water and associated Mn/Fe-oxide crusts from the Clarion Fracture Zone southeast of Hawaii. Abst., JOA Meeting, Edinburgh, 1976.
- Hajash, A., 1975. Hydrothermal processes along mid-ocean ridges: an experimental investigation. *Cont. Miner. Petrol.*, v. 53, p. 205-226.
- Harder, H. and Flehmig, W., 1970. Quarzsynthese bei tiefen Temperaturen. *Geochim. Cosmochim. Acta*, v. 34, p. 295-305.
- Harriss, R. C., 1968. Mercury content of deep-sea manganese nodules. *Nature*, v. 219, p. 54-55.
- Haskin, M. A. and Haskin, L. A., 1966. Rare-earth in European shales: a redetermination. *Science*, v. 154, p. 307-309.
- Hawley, J. E. and Ingle, J. D., Jr., 1975. Improvements in cold vapor atomic absorption determination of mercury. *Anal. Chem.*, v. 47, p. 719-723.
- Heath, G. R. and Dymond, J. R., 1977. Genesis and diagenesis of metal-liferous sediments from the East Pacific Rise, Bauer Deep and Central Basin, northwest Nazca Plate. submitted to *Geol. Soc. Amer. Bull.*
- Hem, J. D. and Skougstad, M. W., 1960. Coprecipitation effects in solutions containing ferrous, ferric and cupric ions. U. S. Geol. Survey Solutions Paper No. 1342.
- Hogdahl, O. T., Melson, S., and Bowen, V. T., 1968. Neutron activation analysis of lanthanide elements in seawater. *Adv. Chem.*, v. 73, p. 308-325.
- Honnorez, J., Jonnoret-Guerstein, B., Valette, J., and Wauschkuhn, A., 1973. Present day formation of an exhalative sulfide deposit at Vulcano (Tyrrhenian Sea), part II: active crystallization of fumarolic sulfides in the volcanic sediments of the Baia di Levante. In: *Ores in Sediments*, ed. G. T. Amstutz and A. J. Bernard, Springer-Verlag, p. 139-166.
- Horn, M. K. and Adams, J. A. S., 1966. Computer-derived geochemical balances and element abundances. *Geochim. Cosmochim. Acta*, v. 30, p. 279-297.
- Horowitz, A., 1970. The distribution of Pb, Ag, Sn, Tl, and Zn in sediments on active oceanic ridges. *Mar. Geol.*, v. 9, p. 241-259.

- Imbrie, J. and Kipp, N. G., 1970. A new micropaleontological method for quantitative paleoclimatology: application to a late Pleistocene Caribbean core, in the late Cenozoic Glacial ages, Yale University Press, New Haven.
- Imbrie, J. and van Andel, Tj. H., 1964. Vector analysis of heavy mineral data. *Geol. Soc. Am. Bull.*, v. 75, p. 1131-1156.
- Klovan, J. E. and Imbrie, J., 1971. An algorithm analysis and calculation of factor scores. *Mathematical Geol.*, v. 3, p. 61-67.
- Krauskopf, K. B., 1956. Factors controlling the concentration of thirteen rare elements in sea water. *Geochim. Cosmochim. Acta*, v. 9, p. 1-32B.
- Krauskopf, K. B., 1957. Separation of manganese from iron in sedimentary processes. *Geochim. Cosmochim. Acta*, v. 12, p. 61-84.
- Lister, C. R. B., 1972. On the thermal balance of a mid-ocean ridge. *Geophys. J. R. Astr. Soc.*, v. 26, p. 515.
- Loganathan, P. and Bureau, R. G., 1973. Sorption of heavy metal ions by a hydrous manganese oxide. *Geochim. Cosmochim. Acta*, v. 37, p. 1277-1293.
- Lyle, M., Dymond, J. R., and Heath, G. R., 1977. Copper-nickel enriched ferromanganese nodules and associated crusts from the Bauer Deep, northwest Nazca Plate. submitted to *Earth Planet. Sci. Lett.*
- MacLean, W. H. and Shimazaki, H., 1976. The partition of Co, Ni, Cu and Zn between sulfide and silicate liquids. *Econ. Geol.*, v. 71, p. 1049-1057.
- Mattinson, J. M., 1972. Preparation of HF, HCl, and HNO₃ at ultra-low Pb levels. *Anal. Chem.*, v. 44, p. 1715-1716.
- Moore, W. S. and Vogt, P. R., 1975. Hydrothermal manganese crusts from two sites near the Galapagos spreading axis. *Earth Planet. Sci. Lett.*, v. 29, p. 349-356.
- Mottl, M. J., Corr, R. F., Holland, H. D., 1974. Chemical exchange between seawater and mid-ocean ridge basalt during hydrothermal alteration: an experimental study. *Geol. Soc. Am.*, 87th Ann. Meet. Abst. with Programs, v. 6, p. 879-880.
- Mottl, M. J., Corr, R., and Holland, H. E., 1975. Trace element content of Reykjanes-Svartsengi thermal brines, Iceland. *Geol. Soc. Am.* 88th Ann. Meet. Abst. with Programs, v. 7, p. 1206.
- Murray, J. W., 1973. The interaction of metal ions with hydrous manganese dioxide in the marine environment. Chapter 5, unpub. Ph.D. Thesis. p. 197-233.

- Murray, D. J., Healy, T. W., and Fuerstenau, D. W., 1968. The adsorption of aqueous metal on colloidal hydrous manganese oxide. *Adv. Chem. Ser.*, v. 79, p. 74-81.
- Onishi, H. and Sandell, E., 1955a. Geochemistry of arsenic. *Geochim. Cosmochim. Acta.*, v. 7, p. 1.
- Onishi, H. and Sandell, E., 1955b. Notes on the geochemistry of antimony. *Geochim. Cosmochim. Acta.*, v. 8, p. 213.
- Piper, D. Z., 1974. Rare earth elements in ferromanganese nodules and other marine phases. *Geochim. Cosmochim. Acta.*, v. 38, p. 1007-1022.
- Piper, D. Z., Veeh, H. H., Bertrand, W. G., and Chase, R. L., 1975. An iron-rich deposit from the Northeast Pacific. *Earth Planet. Sci. Lett.*, v. 26, p. 114-120.
- Raab, W., 1972. Physical and chemical features of Pacific deep sea manganese nodules and their implications to the genesis of nodules. In: *Ferromanganese deposits on the ocean floor*, ed. D. R. Horn. IDOE Publication, p. 31-49.
- Rankama, K., and Sahama, T. G., 1950. *Geochemistry*. Chicago, University Press.
- Rona, P. A., McGregor, P. R., Betzer, P. R., and Krause, D. C., 1974. Anomalous water temperatures over Mid-Atlantic Ridge crest at 26°N (abstract), *EOS Trans. Amer. Geophys. Union*, v. 55, p. 193.
- Scott, M. R., Scott, R. B., Rona, P. R., Butler, L. W., and Nalwalk, A. J., 1974. Rapidly accumulating manganese deposit from the median valley of the Mid-Atlantic Ridge. *Geophys. Res. Lett.*, v. 1, p. 355-358.
- Scott, R. B., Rona, P. A., and McGregor, B. A., 1974. The TAG hydrothermal field. *Nature*, v. 251, p. 301-302.
- Scott, R. B., Malpas, J., Rona, P. A. and Udintsev, G., 1976. Duration of hydrothermal activity at an oceanic spreading center, Mid-Atlantic Ridge (lat. 26°N). *Geology*, v. 87, p. 233-236.
- Seyfried, W., and Bischoff, J. L., 1977. Hydrothermal transport of heavy metals by sea-water: the role of seawater/basalt ratio. Submitted to *Earth Planet. Sci. Lett.*
- Stumm, W. and Morgan, J. J., 1970. *Aquatic chemistry*. Wiley-Interscience.
- Talwani, M., Windisch, C. C., and Langseth, M. G., 1971. Reykjanes Ridge crest: a detailed geophysical study. *J. Geophys. Res.*, v. 76, p. 473-517.

- Tomasson, J. and Kristmannsdottir, H., 1972. High temperature alteration minerals and thermal brines, Reykjanes, Iceland. *Contr. Mineral. and Petrol.*, v. 36, p. 123-134.
- Turekian, K. K. and Wedepohl, K. H., 1961. Distribution of the elements in some major units of the earth's crust. *Bull. Geol. Soc. Amer.*, v. 72, p. 175-192.
- United States Geological Survey, 1970. Mercury in the environment. U. S. Geol. Survey Prof. Paper 713, 67 p.
- Williams, D. L., Von Herzen, R. P., Sclater, J. G., and Anderson, R. N., 1974. The Galapagos Spreading Center: lithospheric cooling and hydrothermal circulation. *Geophys. J. Roy. Astr. Soc.*, v. 38, p. 587-613.
- Zelenov, K. K., 1964. Iron and manganese exhalations from the submarine volcano Banu Wuhu (Indonesia) *Dokl. Akad. Nauk SSSR*, v. 155, p. 1317-1320 (Eng. Trans.).

APPENDICIES

APPENDIX I

Sample Descriptions

HYDROTHERMAL CRUSTS

T3-72D 253-13-21

Samples: MN1749 bulk
 MN1896 surface scrape

Location: TAG Geothermal Field Water Depth: 3400 m
 26°N 45°W

20 mm thick Mn oxide crust. Gray, submetallic luster with laminations 2-5 mm thick. The laminations alternate between soft and porous, dark gray, and hard metallic gray material. The seawater interface is preserved. It is rough and pitted, with tiny botryoids of the metallic material and a thin coating of the soft, dark material inside the cavities.

The surface layer (MN1896) is predominantly the soft, dark material, while the bulk sample (MN1749) is mostly metallic.

This sample was collected at dredge site 13 in the median valley of the MAR during the 1972 Trans-Atlantic Geotraverse (TAG) program. This site is a talus slope at the base of the median valley scarp, 5 kilometers from the valley axis.

TO 75AK61-1A31A, -1A31B, 1A24

Sample Pairs: MN1845 ferromanganese; MN1846 hydrothermal
 MN1847 ferromanganese; MN1848 hydrothermal
 MN1849 ferromanganese; MN1850 hydrothermal

Location: Near TAG Geothermal Field Water Depth: 2500 m
 26°07'N 44°40'W

Three Mn crusts, each consisting of two distinct layers. The basal layers, occurring on altered basalt, are brownish-black, submetallic undulating laminae, up to 10 mm thick, with slightly botryoidal surfaces. These basal layers appear identical to the 72D 13 (TAG) hydrothermal crust. They are overlain by a less than 2 mm thick layer of grayish-black material with highly irregular microbotryoidal surfaces, similar in appearance to ferromanganese coatings. These two crust types were carefully separated for chemical analysis.

APPENDIX I, continued

These crusts were collected 18 kilometers from the rift axis of the MAR as part of the TAG project in spring, 1975.

DS 74 D6

Samples: MN1850 top surface
 MN1851 center metallic layer
 MN1852 bottom surface

Location: Galapagos Spreading Center Water Depth: 1600 m
 02°43'N 95°15'W

15 mm thick Mn oxide crust consisting of a thick, gray banded zone, approximately 10 mm thick, between thin upper and lower layers of very dark gray friable material. The banded zone has metallic luster and individual bands, approximately 1 mm thick, of various shades of gray. This zone is not continuous, but bends and pinches out into the friable material in several locations.

This crust was collected on a northern wall of an axial valley of the Galapagos Spreading Center, about 5 kilometers from the spreading axis.

CYP 74-12 and CYP 74 26-15A

Samples: MN1776 Mn-rich crust
 MN1777 Fe-rich crust

Location: FAMOUS Site Water Depth: 2670 m
 36°56'N 33°04'W

Massive, friable dark gray and brownish gray crusts covered with calcareous ooze. Veins of friable dark gray and orange-brown material can be seen in some pieces of the crusts.

These samples were collected by the French submersible Archimede during the French-American Mid-Ocean Undersea Study (FAMOUS) in the summer of 1974. They were part of a large deposit surrounding visible hydrothermal vents. This was the first in situ observation and sampling of such a deposit on the ocean floor. The location of this deposit is near the summit of a scarp which forms the southern wall of the active portion of the transform valley of fracture zone A. It covers an area of about 40 by 15 meters and is generally 10 to 50 cm thick, but up to 1 m thick near the main vent. The Fe/Mn ratio of this large deposit is highly variable, changing from iron-rich near the vent to manganese-rich several meters away.

APPENDIX I, continued

Two samples of this crust were analyzed; one iron-rich and one manganese-rich.

IOUBC 70-16-12D

Sample: MN1775

Location: Dellwood Seamount, N.E. Pacific Water Depth: 600-800 m
50°45.7'N 130°53.0'W

Fragments up to 10 mm thick of yellowish-red, thinly layered, semi-consolidated material. Layers are on the order of 1 mm thick and of slightly different shades of yellow-red. The layers are undulating and bent, possibly due to deposition on an irregular bottom (Piper et al., 1975).

FERROMANGANESE COATINGS

Y74-1-1DR 8

Sample: MN1659

Location: Juan de Fuca Ridge Water Depth: 2169 m
45°46'N 130°01'W

1-3 mm thick grayish-brown coating on an altered basalt pillow fragment.

Y74-1-3DR 26

Sample: MN1626

Location: Juan de Fuca Ridge Water Depth: 1250 m
45°27'N 130°08'W

1-5 mm thick dark gray friable coating covering the glassy surface of a highly altered basalt pillow fragment.

APPENDIX I, continued

Y74-1-3DR 31

Sample: MN1660

Location: Juan de Fuca Ridge Water Depth: 1250 m
 45°27'N 130°08'W

1-2 mm thick dark grayish-brown coating on a basaltic pillow fragment.

Y74-1-6DR 40

Y74-1-6DR 59

Sample: MN1627

MN1630

Location: Juan de Fuca Ridge Water Depth: 2251 m
 44°45'N 130°17'W

1-3 mm thick very dark grayish brown coatings on large, partially palagonized basaltic glass fragments.

Y73-4-48DR 3

Sample: MN1657

Location: East Pacific Rise Water Depth: 1938 m
 18°44'S 140°56'W

1-2 mm dark brown coating covering glassy and highly palagonized surface of an altered basalt pillow fragment.

Y73-3-22DR

Sample: MN1194

Location: Bauer Basin Water Depth: 4435 m
 13°40'S 102°09'W

Fragments of dense, dark brownish gray coating up to 15 mm thick. It is very hard with resinous luster and little internal structure. The top surface is characterized by micro-botryoidal texture.

APPENDIX I, continued

Y74-1-10DR 9

Samples: MN1628 whole crust
 MN1629 surface layer

Location: Seamount, N.E. Pacific Water Depth: 2801 m
 36°51'N 125°56'W

Large fragments of dark gray massive coating up to 25 mm thick. It is soft and completely non-metallic, having a texture similar to semi-consolidated clay. A 1-4 mm thick darker surface layer is distinguishable and appears to be the most recent depositional phase. It has a surface that is generally smooth but with some micro-botryoidal texture.

MANGANESE NODULES

SOTW 34D

Sample: MN1468

Location: East Pacific Rise Water Depth: 3611 m
 12°44'S 113°35'W

Dark brown, very porous nodule. Its external surface is pitted overall and botryoidal in one area. Internally it contains abundant large and small cavities. Concentric layering is present but indistinct.

Y73-3-22D

Sample: MN1188

Location: Bauer Basin Water Depth: 4435 m
 13°40'S 102°09'W

Small, dark gray, ellipsoidal nodule, about 4 cm in diameter. Its internal layering indicates that it has formed by over-growth around an older nodule fragment.

APPENDIX I, continued

DR9/SM

Sample: MN1641

Location: N. Equatorial Pacific Water Depth: 3000 m
 18°18'N 161°46'W

MP 4300

Sample: MN1642

Location: N. Equatorial Pacific Water Depth: 1800 m
 11°57'N 164°59'W

Dark gray powdered samples received from D. Z. Piper.

GRLD 126

Sample: MN1763

Location: Equatorial Pacific

Kennecott standard manganese nodule.

IMPREGNATED SEDIMENT

VA 13/1

Samples: MN1809 0-4 mm
 MN1810 4-8 mm
 MN1811 8-12 mm

Location: Clarion Fracture Zone Water Depth: 5739 m
 13°59.5'N 152°59.0'W

A 12 mm thick section of semi-consolidated sediment which appears to have been baked and impregnated with manganese and iron oxides. The top surface is completely oxide covered, with a micro-botryoidal texture. This crust penetrates down into the sediment in numerous small veins. The 0-4 mm section (MN1809) is nearly pure crust material; 4-8 mm (MN1810) is sediment with numerous veins; 8-12 mm (MN1811) is mostly sediment material with few veins.

This sample was collected from the Clarion Fracture Zone at a station where the bottom water temperature was reported to be greater than 20°C (Gundlach et al., 1976).

APPENDIX II. RESULTS OF CHEMICAL ANALYSES. HYDROTHERMAL CRUSTS

	MN1749	MN1895	MN1846	MN1848	MN1850	MN1750	MN1751	MN1752	MN1776	MN1777	MN1775
	TAG	TAG	TAG	TAG	TAG	GSC	GSC	GSC	FAMOUS	FAMOUS	JSM
MAJOR ELEMENTS (PERCENT)											
FE	.13	.12	.21	.14	.2	.21	.1	.29	6.77	25.39	38.1
MN	41.	8.42	44.2	44.2	43.25	52.5	49.3	43.8	31.	4.49	1.5
SI	.12	--	1.	.87	.86	.04	.16	.28	4.72	19.38	9.16
AL	.07	--	--	.43	.04	.05	.02	.16	.55	.02	.01
MINOR ELEMENTS (PPM)											
CO	5.5	--	48.5	31.8	35.8	9.5	.6	5.4	33.	5.1	2.9
NI	4.3	34.3	2200.	782.6	624.	67.	45.	537.	163.	6.	40.
CU	16.	11.	1129.	555.	427.	88.	15.3	240.	142.3	9.3	2.6
ZN	195.	87.	1448.	468.	564.	495.	598.	445.	172.4	13.5	61.
BA	400.	--	--	1010.	946.	60.	130.	330.	1060.	80.	141.
VOLATILE ELEMENTS (HG=PPM AS,SB,P3=PPM)											
HG	500.	1040.	740.	314.	510.	110.	40.	296.	159.	136.	3.
AS	53.	--	--	10.	13.	27.4	17.1	13.9	86.	37.3	334.
SB	20.5	--	107.	157.	150.	14.6	17.7	67.	25.3	2.85	6.8
P3	4.	2.	17.	3.8	1.	7.	6.	33.	.7	3.	2.
RARE EARTH ELEMENTS (PPM)											
LA	3.4	--	10.1	4.	5.1	1.4	1.1	4.50	6.7	1.3	1.42
CE	1.7	--	5.8	.5	.7	.5	.5	1.40	9.2	.3	.2
SM	1.1	--	2.	.93	1.1	2.9	2.5	4.20	3.3	.36	2.54
EU	.17	--	6.23	.29	2.35	.15	.07	.28	.4	.06	.04
TB	.10	--	.37	.19	.12	.13	.04	.18	.1	.03	.06
YB	1.	--	1.8	1.4	1.	.4	.1	.60	.4	1.2	.4
LU	.14	--	.27	.18	.24	.1	.04	.33	.1	.32	.87

APPENDIX II CONTINUED. FERROMANGANESE COATINGS

	MN1659	MN1626	MN1660	MN1627	MN1631	MN1657	MN1194	MN176A	MN1623	MN1629
	JDF	JDF	JDF	JDF	JDF	EPR	BO	MAR	SM	SM
MAJOR ELEMENTS (PERCENT)										
FF	16.9	19.2	18.48	19.86	20.55	27.09	23.88	26.3	30.7	23.49
MN	10.4	12.32	11.	13.69	12.65	4.84	17.79	10.27	8.11	6.8
SI	10.	12.62	12.5	13.56	11.9	6.55	5.46	4.45	9.27	14.5
AL	2.07	2.72	2.97	2.27	2.45	1.47	1.49	3.43	1.22	2.37
MINOR ELEMENTS (PPM)										
CO	490.	444.	411.	316.	260.	157.8	1420.	3430.	1740.	1550.
NI	1730.	1471.	1530.	1780.	1690.	519.	3790.	1043.	1950.	1097.
CU	270.	340.7	324.	551.3	448.	930.	1736.	1169.	906.	442.
ZN	370.	493.	253.	680.	590.	632.	632.	485.	812.5	610.
BA	1390.	1670.	1240.	1873.	1911.	820.	1670.	754.	2047.	1430.
VOLATILE ELEMENTS (HG=PPB AS,SP,PR=PPM)										
HG	182.	125.	88.	62.	210.	300.	20.	13.	72.	49.
AS	234.	279.	177.	105.	189.	309.	394.	710.	273.	284.
SA	21.4	19.	10.7	20.2	21.3	28.3	46.7	151.	93.	31.7
PR	215.	221.	149.	250.	193.	30.	200.	333.	2410.	1140.
RARE EARTH ELEMENTS (PPM)										
LA	174.	164.	146.	151.	147.	236.	246.	273.	462.	209.
CF	207.	230.	208.	155.	149.	82.1	182.	963.	1730.	807.
SM	37.5	35.4	30.9	35.1	31.9	12.2	43.6	62.5	82.	44.3
FU	10.9	3.63	0.6	1.74	0.67	2.4	10.4	12.8	2.34	12.3
TO	5.5	5.1	4.77	4.82	4.54	4.03	7.4	6.2	9.	4.52
VR	24.	22.7	21.7	26.5	22.7	12.9	22.9	29.	27.4	18.1
LU	3.95	3.69	3.94	3.83	3.25	2.77	4.34	1.44	3.54	1.82

APPENDIX II CONTINUED. MANGANESE NODULES

	MN1163	MN1188	MN1641	MN1642	MN1763
	EPF	30	N PAC	N PAC	STD NON
MAJOR ELEMENTS (PERCENT)					
FF	31.66	8.26	22.33	16.42	10.32
MN	11.03	33.8	14.53	22.7	24.2
SI	5.26	3.67	5.58	4.08	7.5
AL	.9	1.36	1.03	.85	2.42
MINOR ELEMENTS (PPM)					
CO	475.	686.	4546.	11400.	1560.
NI	1237.	13580.	1882.7	4849.	9670.
CU	1714.	8010.	719.	587.9	6290.
ZN	797.	2390.	614.	693.	1365.
BA	1500.	3710.	2123.	1452.	2430.
VOLATILE ELEMENTS					
(HG=PPM AS,SB,PR=PPM)					
HG	92.	20.	40.	36.	45.
AS	283.	95.	540.	216.	127.
SB	60.	72.	55.	44.4	58.
PR	229.	200.	2370.	2490.	414.
RARE EARTH ELEMENTS (PPM)					
LA	156.	73.4	481.	254.	152.
CF	76.8	74.2	1400.	1140.	590.
SM	23.8	14.3	141.	52.5	38.4
EU	7.59	4.8	27.3	9.66	1.07
TR	5.2	2.94	9.3	1.28	3.23
YB	21.2	13.7	20.3	13.4	17.8
LU	3.5	2.63	1.22	--	6.47

APPENDIX II CONTINUED. FERROMANGANESE IMPREGNATED SEDIMENT AND AMPH D6 SAMPLES

	MN1809	MN1810	MN1811	MN1727	MN1728
	IMP SED	IMP SED	IMP SED	AMPH D6	AMPH D6
MAJOR ELEMENTS (PERCENT)					
FE	10.74	7.67	8.37	22.0	29.9
MN	7.24	6.92	1.16	19.93	1.27
SI	15.73	16.22	21.45	1.08	18.98
AL	5.22	6.12	7.	.58	.99
MINOR ELEMENTS (PPM)					
CO	1320.	--	--	6840.	231.
NI	3850.	3940.	591.	3360.	648.
CU	2790.	3207.	718.	2198.	608.
ZN	447.	385.	180.6	98.	49.
BA	220.	180.	154.	2300.	91.
VOLATILE ELEMENTS					
(HG=PPM AS, SB, PB=PPM)					
HG	62.	--	--	1280.	10.
AS	49.5	--	--	431.	228.
SB	17.4	--	--	0.	31.9
PB	147.	--	--	2037.	92.
RARE EARTH ELEMENTS (PPM)					
LA	38.7	--	--	259.	94.
CE	134.	--	--	1260.	50.9
SM	14.5	--	--	48.4	10.0
EU	4.33	--	--	9.16	2.3
TR	7.92	--	--	1.69	2.24
YB	7.9	--	--	12.7	2.24
LU	.59	--	--	.19	1.79

APPENDIX III

Mercury Analysis of U.S.G.S. Standard Rock GSP-1

This Paper:

Mean: 34 ppb

Range: 31-36 ppb

Standard Deviation: 3

Number of Analyses: 3

U.S.G.S., 1970:

Mean: 22 ppb

Range: 15-41 ppb

Standard Deviation: 11

Number of Analyses: 5 laboratories